CHAPTER-5

RESULTS AND DISCUSSION

5. 1 Results of Elimination of Baseline Wanders Noise for European ST-T and MIT-BIH database using Savitzky-Golay filter

E lectrocardiogram (ECG) is a tool used for the electrical analysis of the status of human heart activity. When the ECG signal is recorded, it gets contaminated with different types of noises. So, noises must be eliminated from the ECG signal for accurate analysis. Other kinds of noises contaminate the characteristics of ECG signal, i.e., Power line interference, baseline wander, Electromyogram (EMG). In this research work, different techniques have been implemented to remove noises. A median filter is used to remove the DC component, and the Savitzky-Golay filter (SG) is used for smoothing noised waveform. Then, wavelet transform (db4) decomposes the ECG signal to remove various artifacts. Wavelet transform provides the information in frequency and time domain, and then thresholding has been applied to implement algorithms in MATLAB. The measured results, i.e., SNR (Signal to Noise ratio) and MSE (Mean square error), have been calculated using different databases like MIT-BIH, European ST-T database. The results are examined with proposed methods that are better than those reported in the literature. Whenever the baseline wander artifact present in an electrocardiogram (ECG) waveform, the waveform diverted from the zero-base line instead of straight line. Incorrect electrode placement, patient mobility, and respiration contribute to this artifact. This artifact in the electrocardiogram (ECG) signal has a negative impact and makes electrocardiogram (ECG) signal detection difficult. This artifact has a frequency range of 0.5 to 1 Hz. To remove baseline wandering noise, we collected 15000 ECG record samples of all records of the MIT-BIH database of 360 Hz sampling frequency and all records of the European ST-T dataset of 250 Hz sampling frequency.

The electrocardiogram (ECG) signal is fragmented to the 10^{th} level into approximation coefficient and detail co-efficient in this proposed work [A. Kumar and M. Singh, 2015]. As a result, the last approximate coefficients, A_9 and A_{10}, which contain the frequency of baseline wander, are set to zero. Figure 5.1, 5.2, Figure 5.3, Figure 5.4, Figure 5.5 shows the removal of the baseline artifact for the European ST-T database Figure 5.6, Figure 5.7….. Figure 5.16 shows the removal of the baseline

artifact for the MIT-BIH database, a short-wavelength artifact that alters the DC component up and down. First, to remove low-frequency noise, subtract the average of the electrocardiogram (ECG) signal from the applied input signal with a one-stage median filter, then smooth the waveform with a Savitzky-Golay filter. The wavelet transform (db_4) is then implemented to the ECG signal to divide it into detail (Cd_1, Cd_2,..., Cd_{10}) and approximate (Ca_1, Ca_2,..., Ca_{10}) coefficients up to the tenth level.

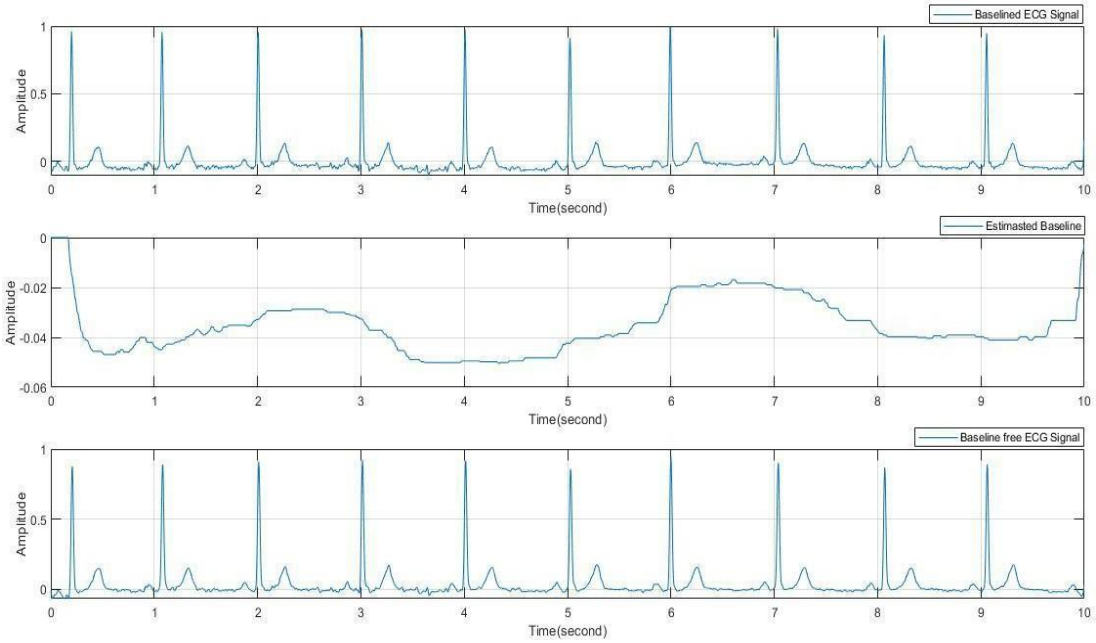

Figure 5.1 Elimination of baseline wanders noise in EDB dataset in e0103 record

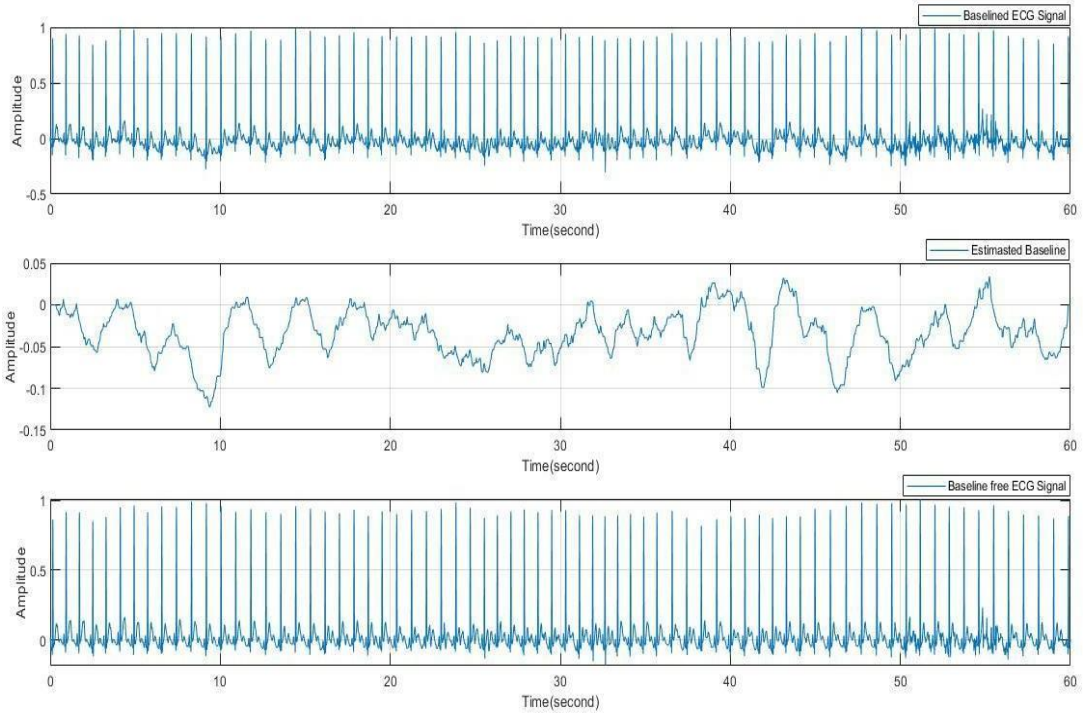

Figure 5.2 Elimination of baseline wanders noise in EDB dataset in e0104 record

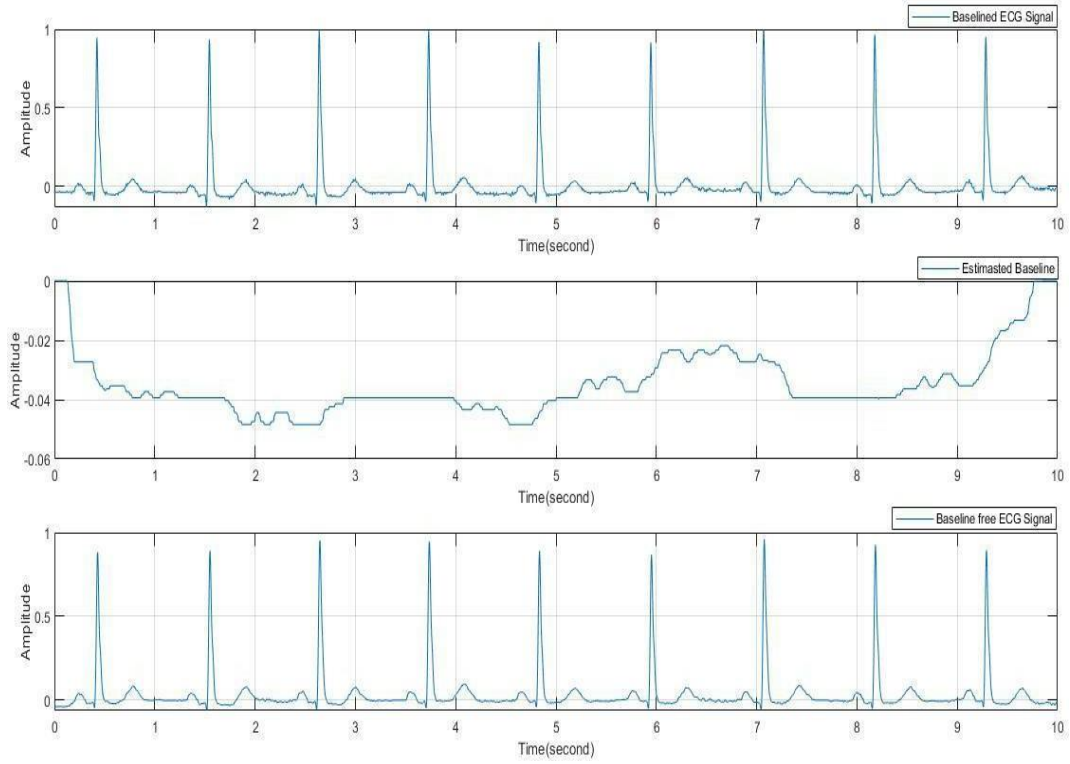

Figure 5.3 Elimination of baseline wanders noise in EDB dataset in e0105 record

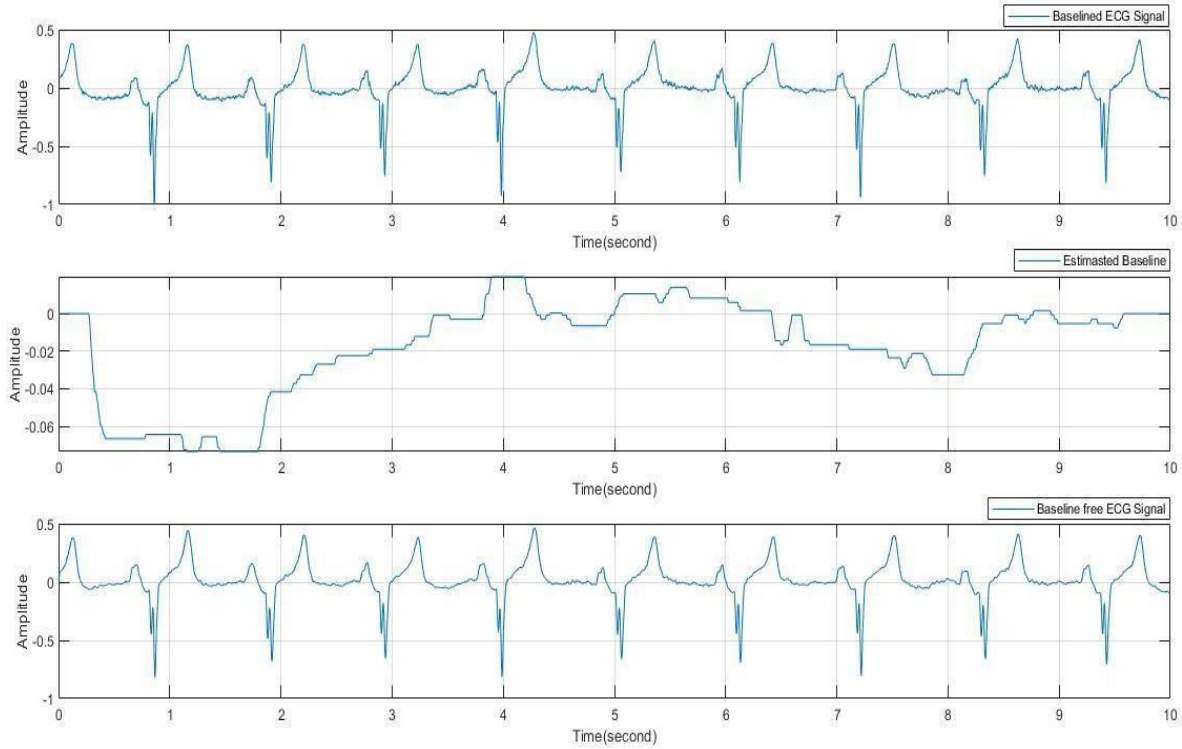

Figure 5.4 Elimination of baseline wanders noise in EDB dataset in e0106 record

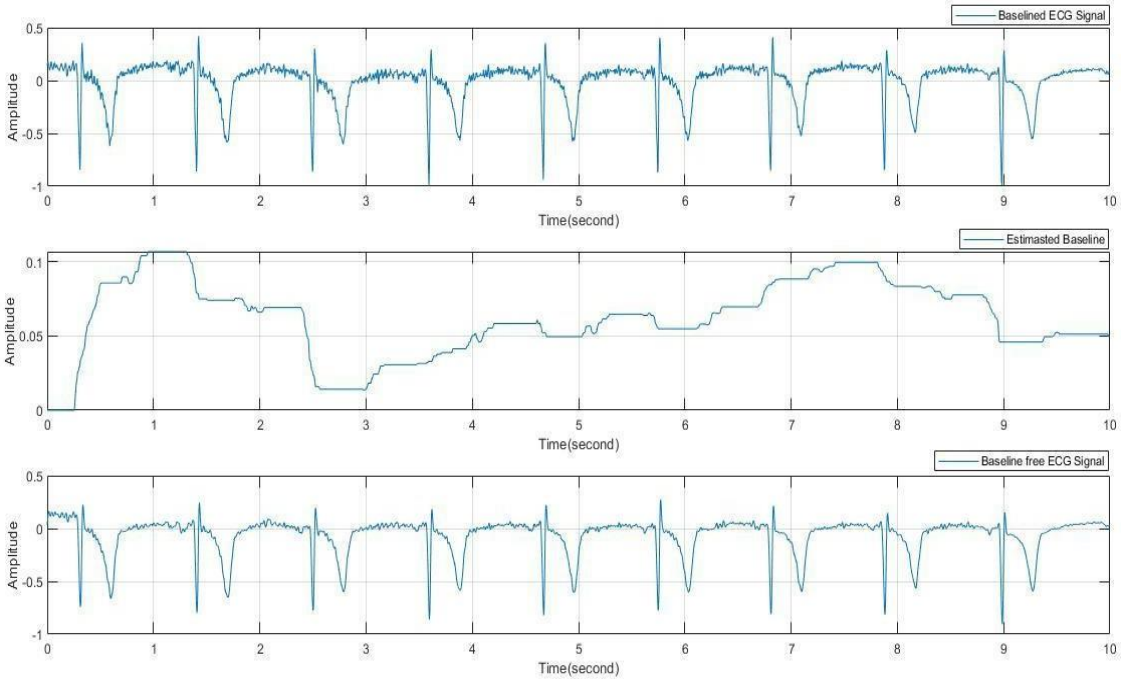

Figure 5.5 Elimination of baseline wanders noise in EDB dataset in e0107 record

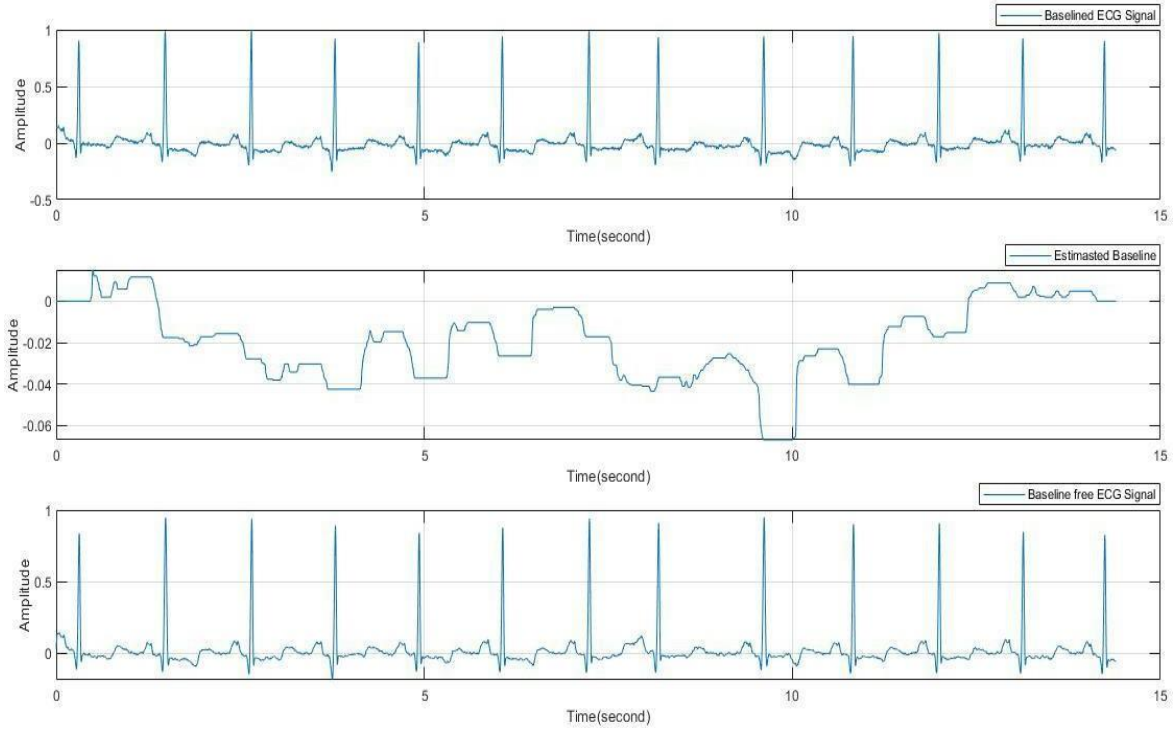

Figure 5.6 Elimination of baseline wanders of MIT-BIH dataset in 100 records

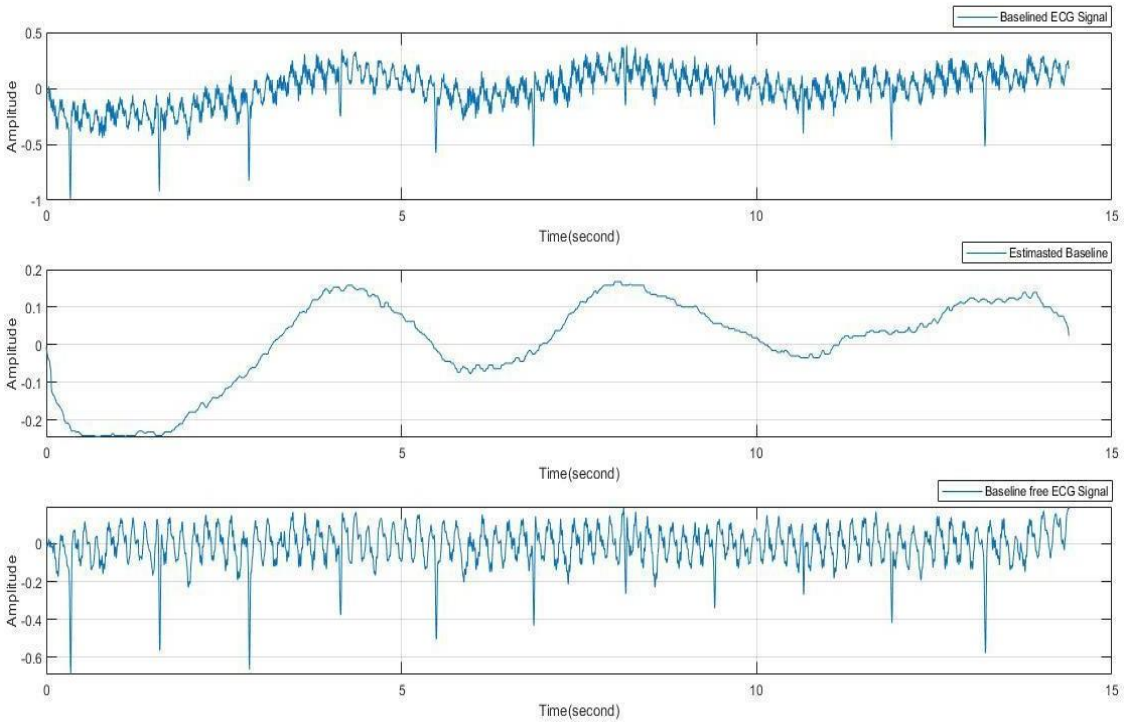

Figure 5.7 Elimination of baseline wanders of MIT-BIH dataset in 101 records

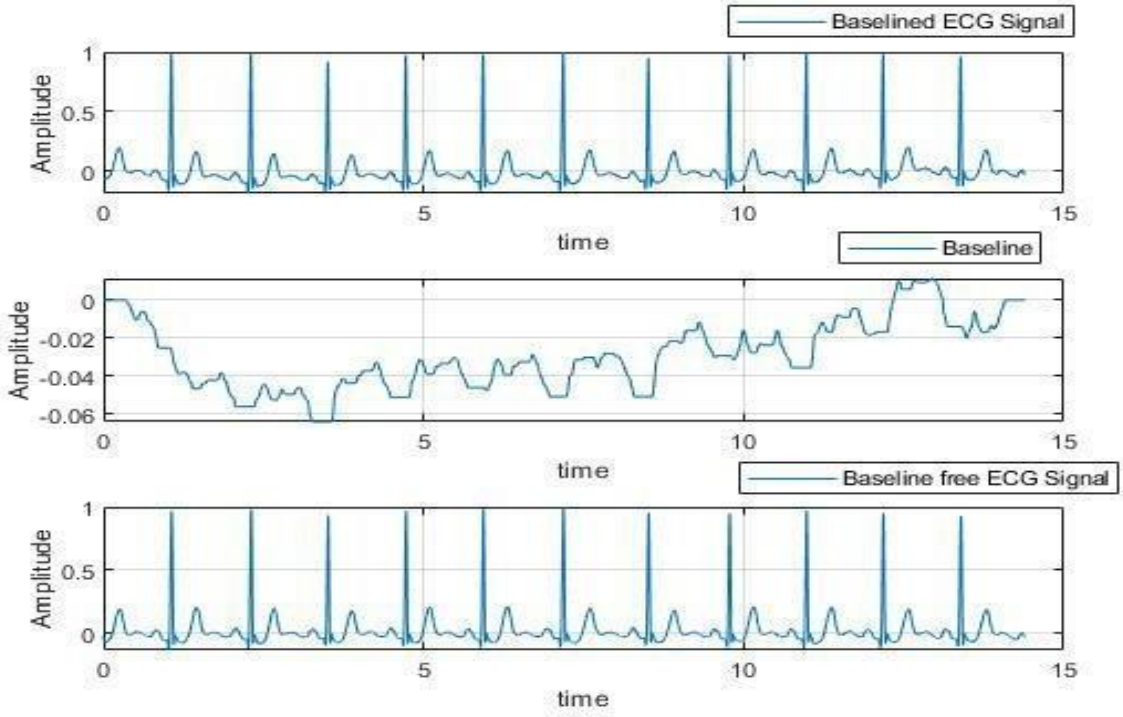

Figure 5.8 Elimination of baseline wanders of MIT-BIH dataset in 103 records

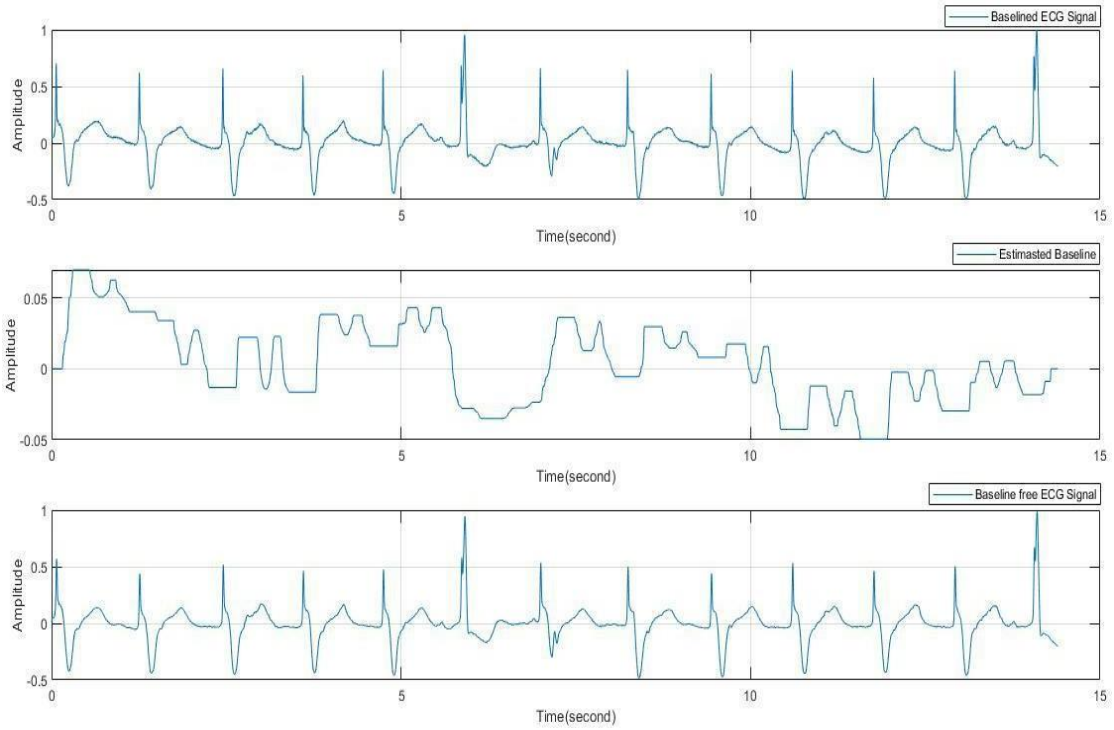

Figure 5.9 Elimination of baseline wanders of MIT-BIH dataset in 104 records

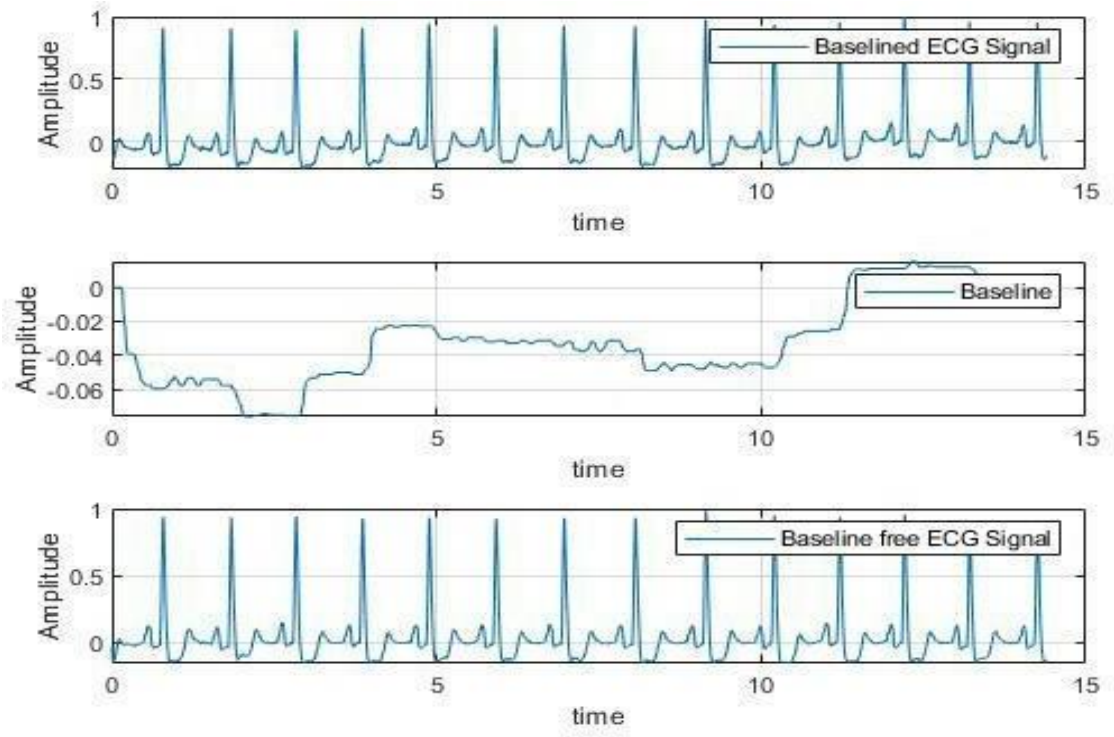

Figure 5.10 Elimination of baseline wanders of MIT-BIH dataset in 105 record

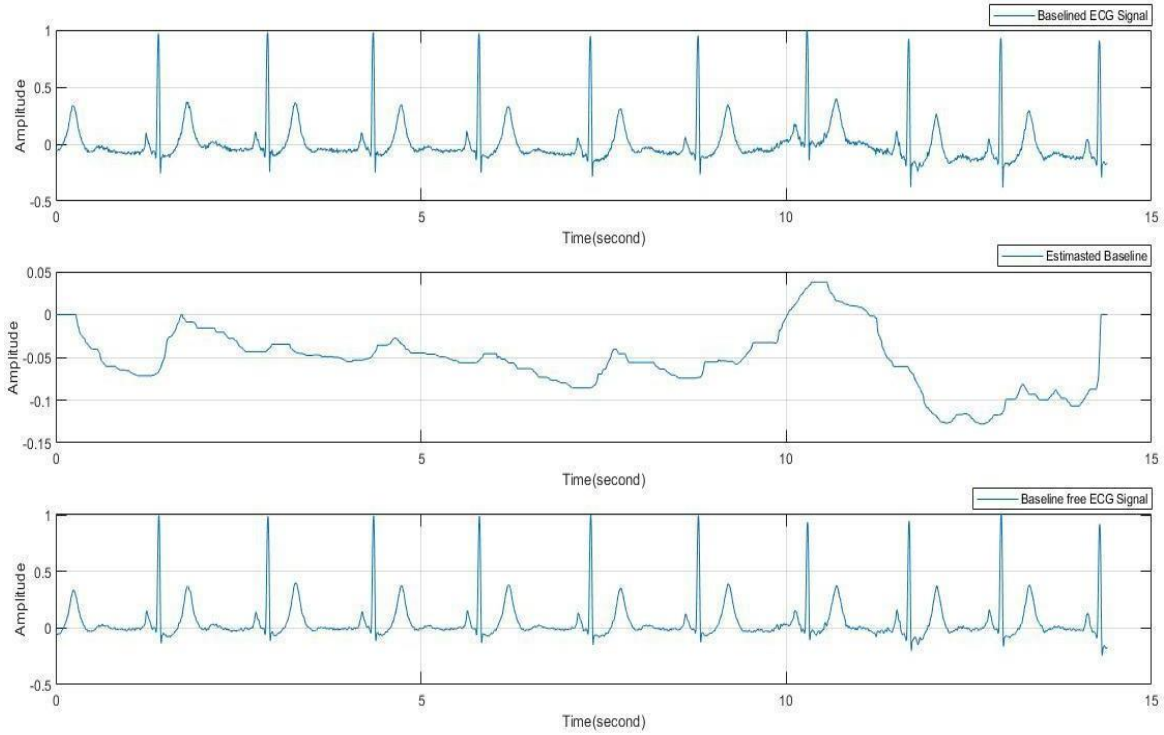

Figure 5.11 Elimination of baseline wanders of MIT-BIH dataset in 106 record

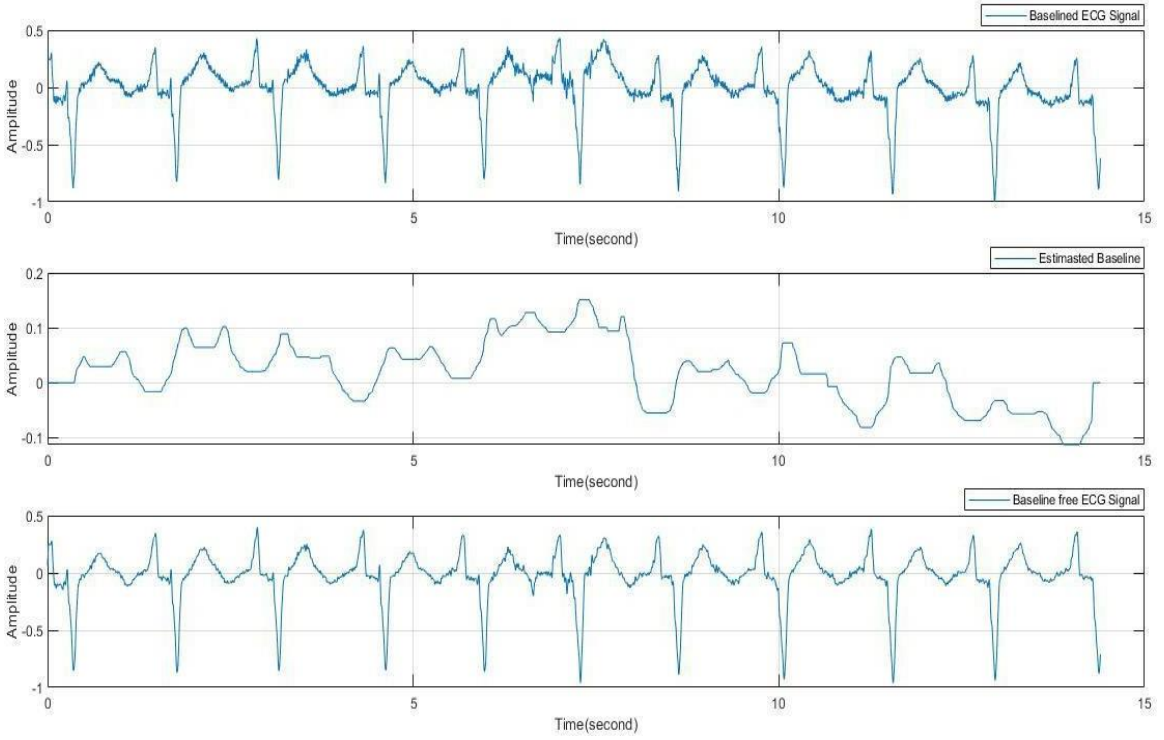

Figure 5.12 Elimination of baseline wanders of MIT-BIH dataset in 108 record

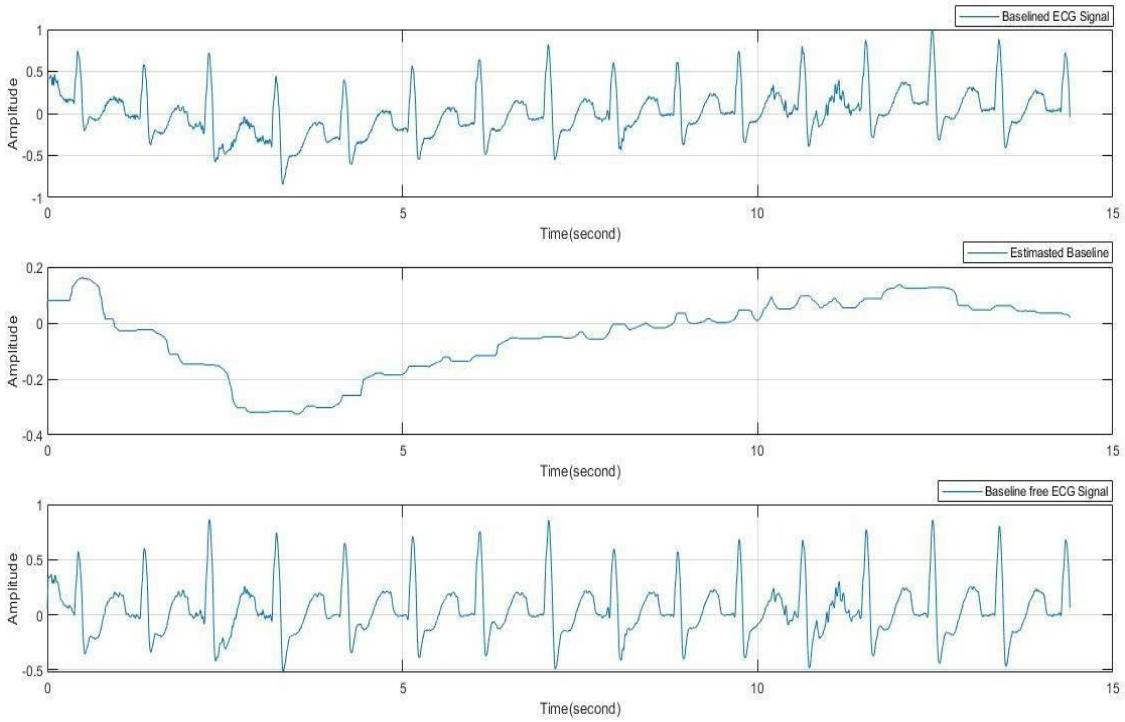

Figure 5.13 Elimination of baseline wanders of MIT-BIH dataset in 112 record

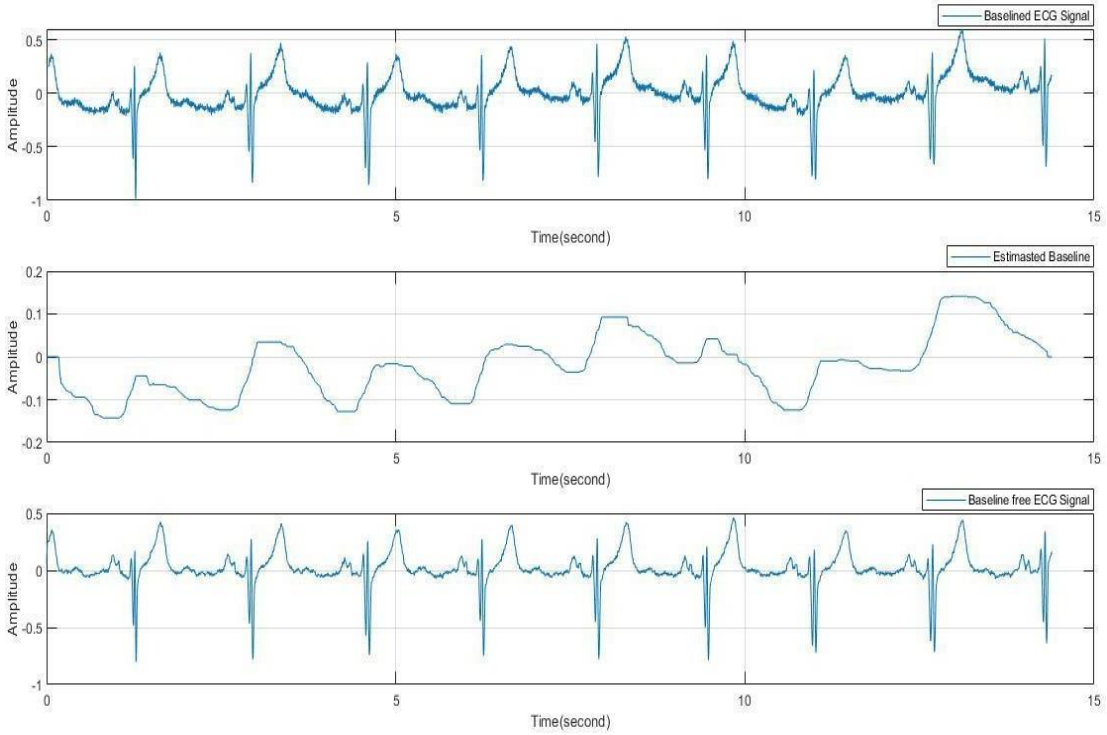

Figure 5.14 Elimination of baseline wanders of MIT-BIH dataset in 114 record

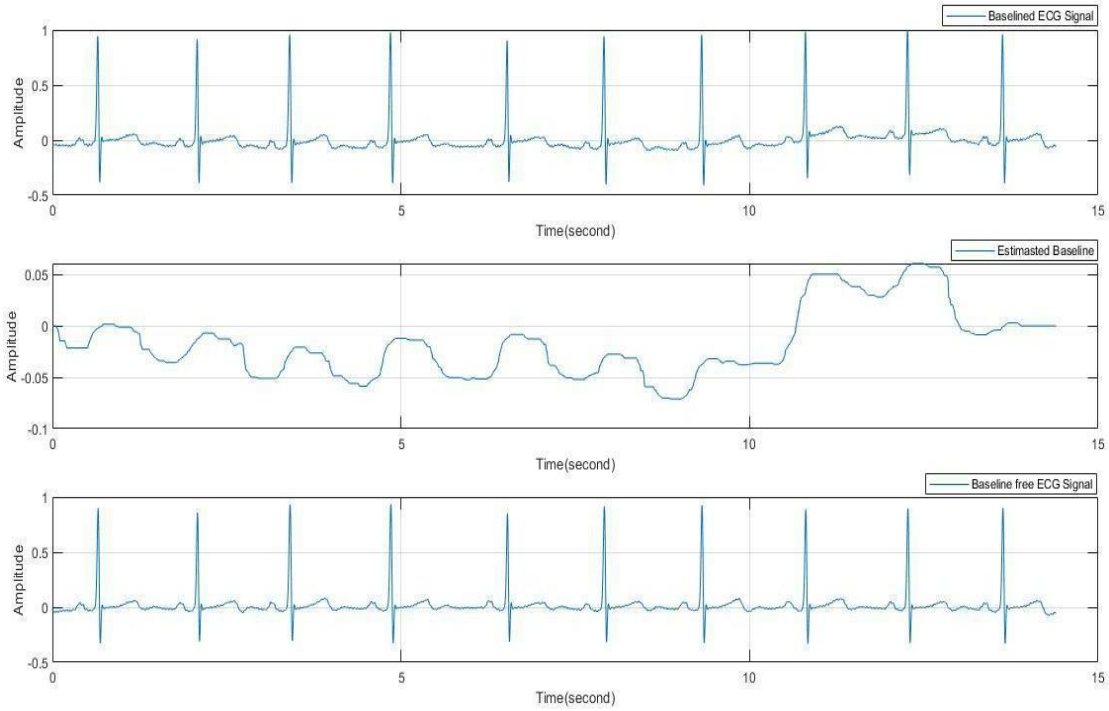

Figure 5.15 Elimination of baseline wanders of MIT-BIH dataset in 115 record

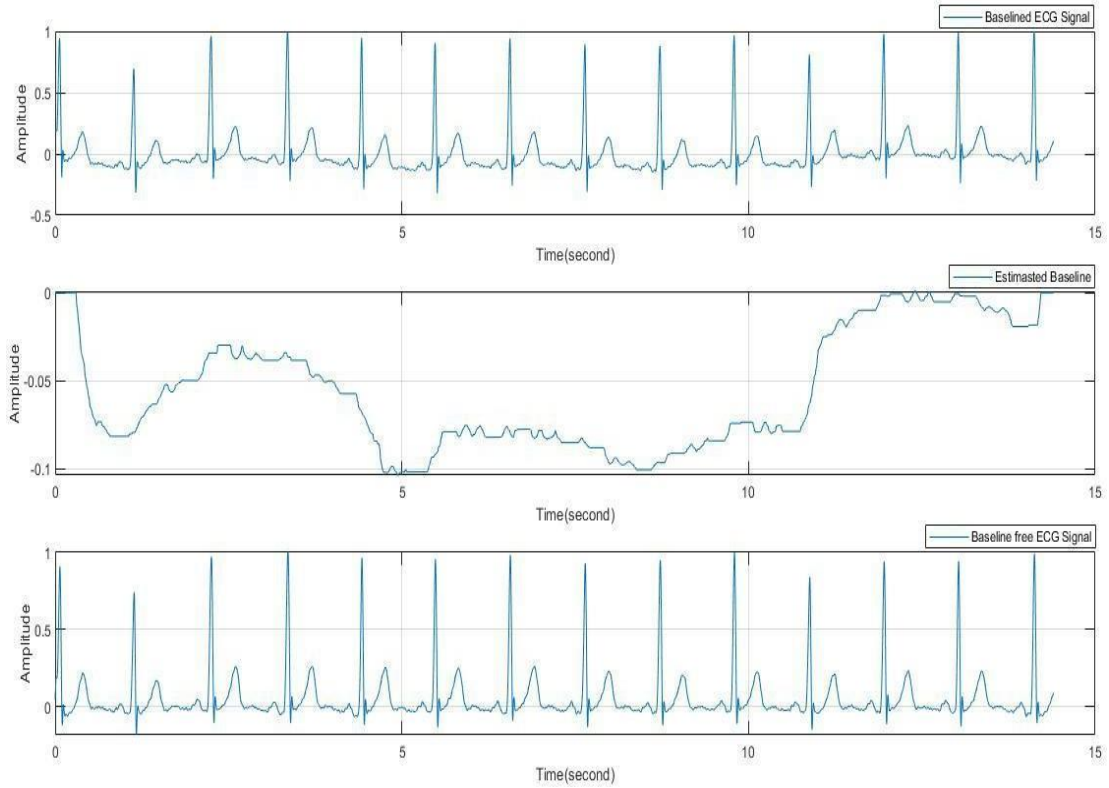

Figure 5.16 Elimination of baseline wanders of MIT-BIH dataset in 116 record

5.2 Elimination of High-frequency noise in ECG signals for European ST-T and MIT-BIH database using MOWPT

As was already mentioned, the artifacts negatively impact the automated characterization of the ECG. For avoidance of mis-detection, unnecessary testing, and medical approaches, it is essential to identify artifact frequencies and distinguish these artifact changes from original changes. Similar to how baseline wandering can impact ST segments in an ECG signal, either ST segment depression or elevation can happen, which might be misinterpreted for myocardial ischemia. We have taken 15000 samples of electrocardiogram records from all records of the MIT-BIH database of 360 Hz sampling frequency to remove high-frequency noise and all records of the European ST-T database with a sample rate of 250 Hz. During recording, high-frequency noise overlaps the features of the electrocardiogram (ECG) signal making electrocardiogram (ECG) signal analysis challenging for even the most experienced specialists. High noise has a frequency range of 100 to 150 Hz. A suitable band pass filter will not effectively minimize this type of noise. As a result, the wavelet transform function is utilized to eliminate high-frequency noise. As a result, the last approximate coefficients, A9 and A10, which contain the frequency of baseline wander, are set to zero. Figure 5.1, Figure 5.2, Figure 5.3, Figure 5.4, and Figure 5.5 shows the removal of the baseline artifact for the European ST-T database and Figure 5.6, Figure 5.7….. Figure 5.16 shows the removal of the baseline artifact for the MIT-BIH database, a short-wavelength artifact that alters the DC component up and down. First, remove low-frequency noise, subtract the average of the electrocardiogram (ECG) signal from the applied input signal with a one-stage median filter, and then smooth the waveform with a Savitzky-Golay filter. The wavelet transform (db4) is then implemented to the ECG signal to divide it into detail (Cd_1, Cd_2,..., Cd_{10}) and approximate (Ca_1, Ca_2,..., Ca_{10}) coefficients up to the tenth level. The coefficients Cd1, and Cd2, which contain high-frequency noise, are thus removed using wavelet. Figure 5.17, Figure 5.18, Figure 5.19, Figure 5.20, Figure 5.21 shows the removal of high-frequency noise European ST-T database and Figure 5.22, Figure 5.23, …. Figure 5.32 shows the removal of high-frequency noise for MIT-BIH database.

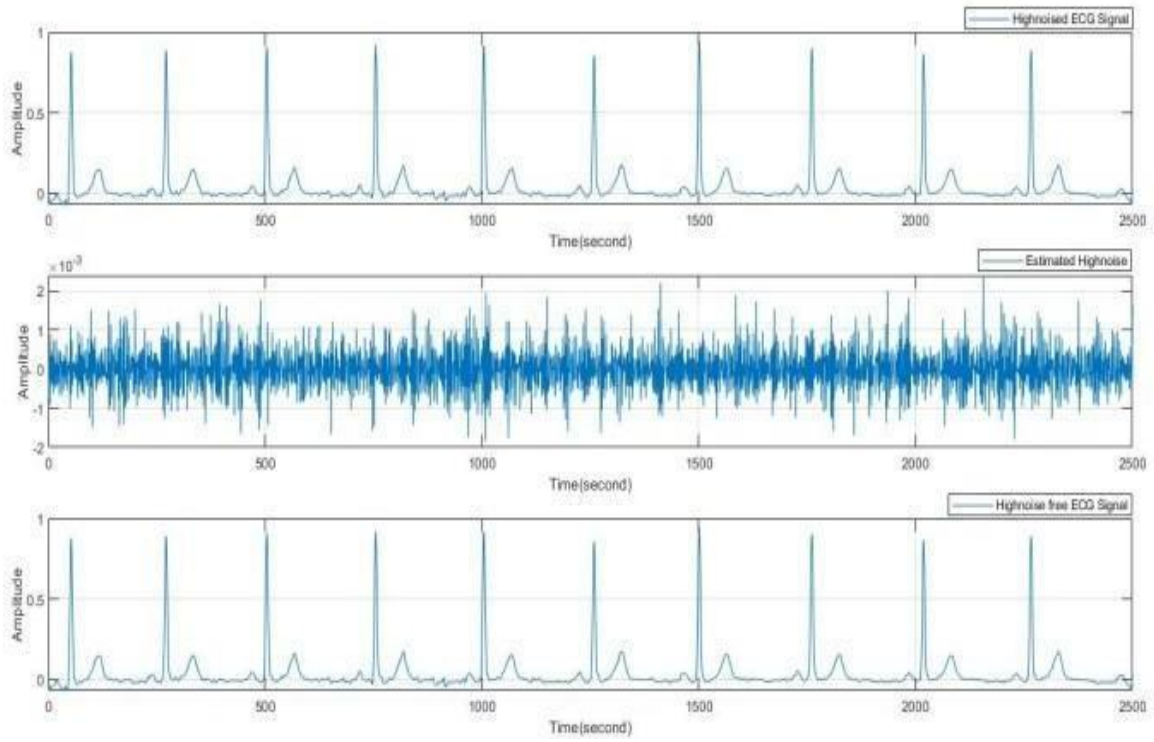

Figure 5.17 Elimination of High-frequency noise of EDB dataset in e0103 record

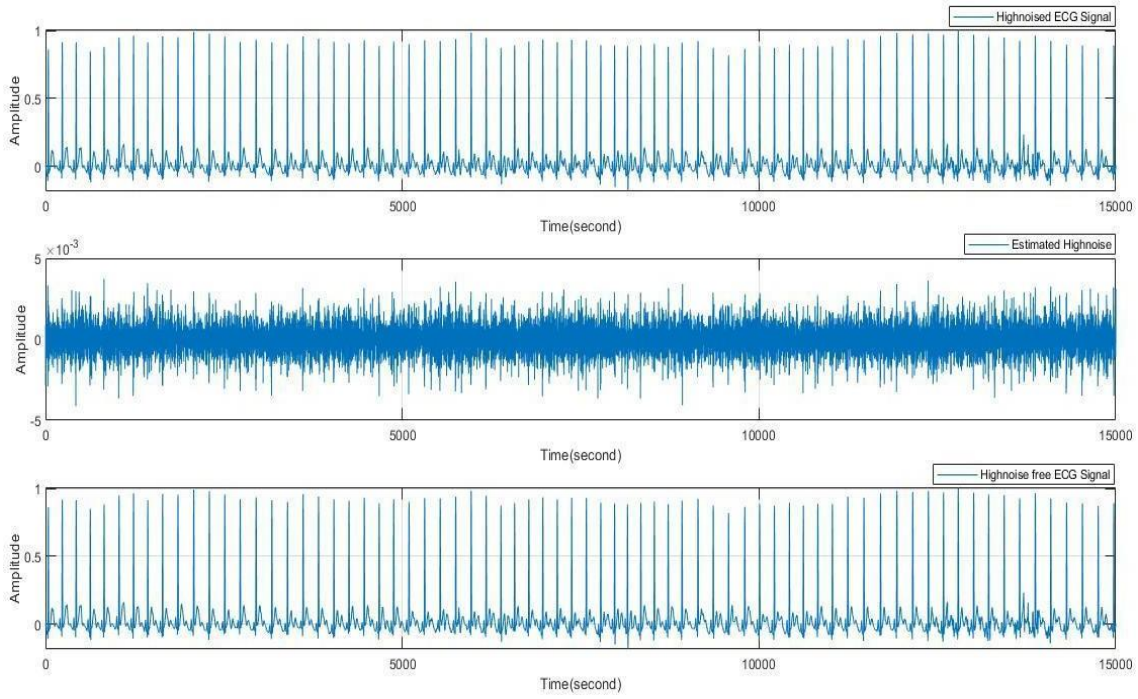

Figure 5.18 Elimination of High-frequency noise of EDB dataset in e0104 record

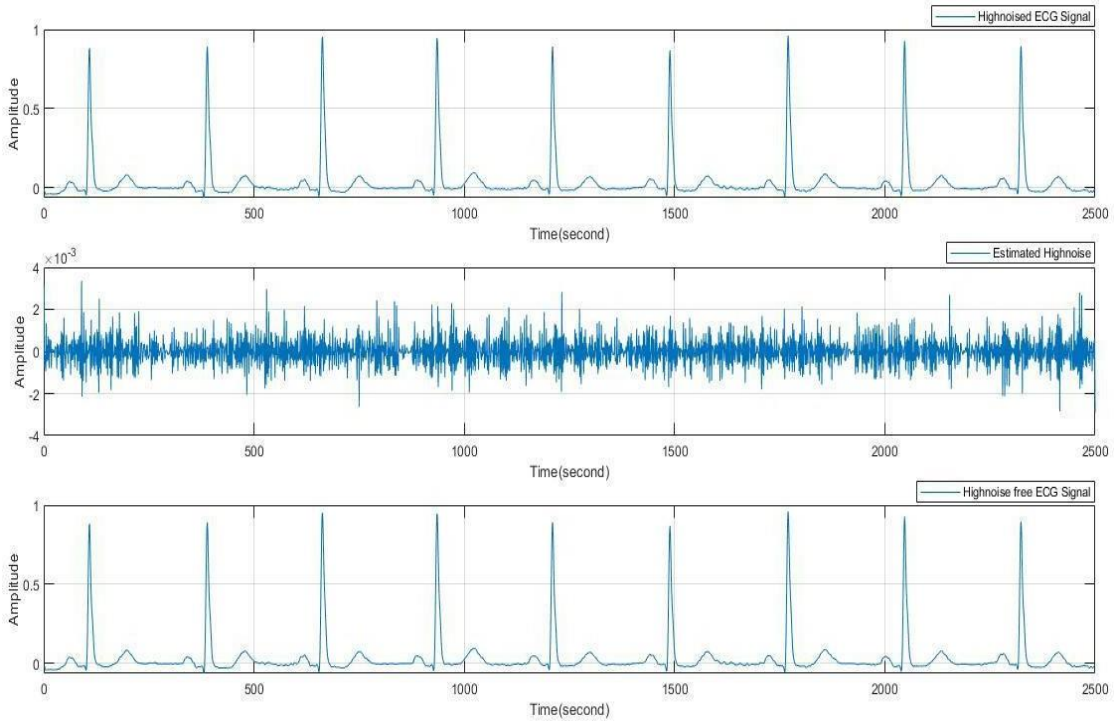

Figure 5.19 Elimination of High-frequency noise of EDB dataset in e0105 record

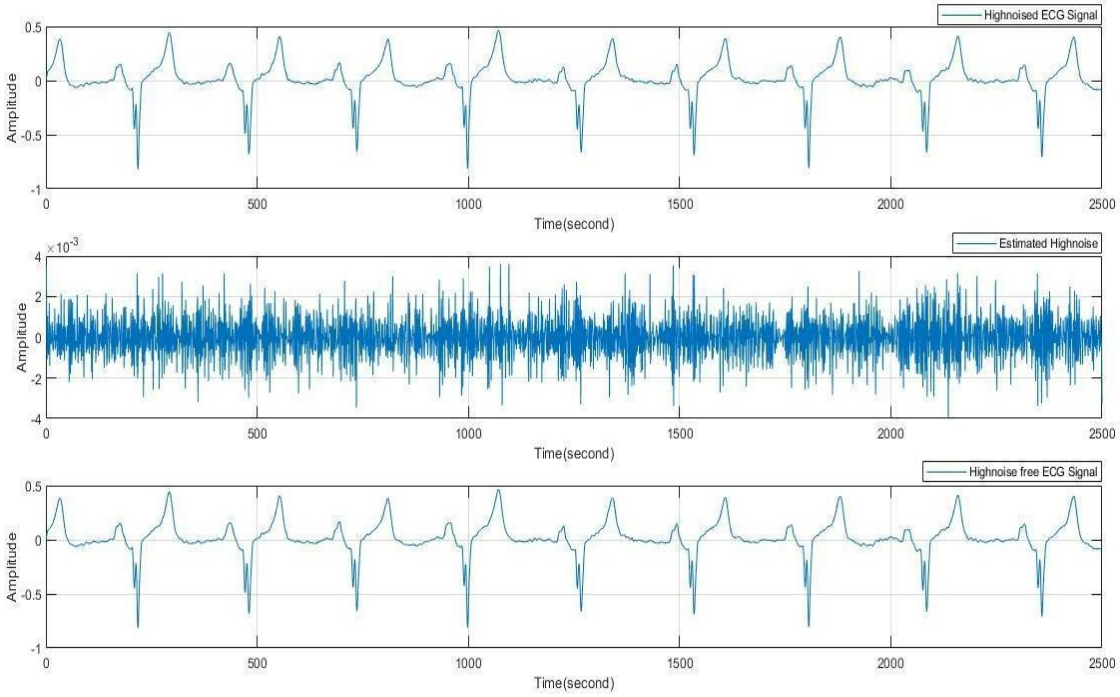

Figure 5.20 Elimination of High-frequency noise of EDB dataset in e0106 record

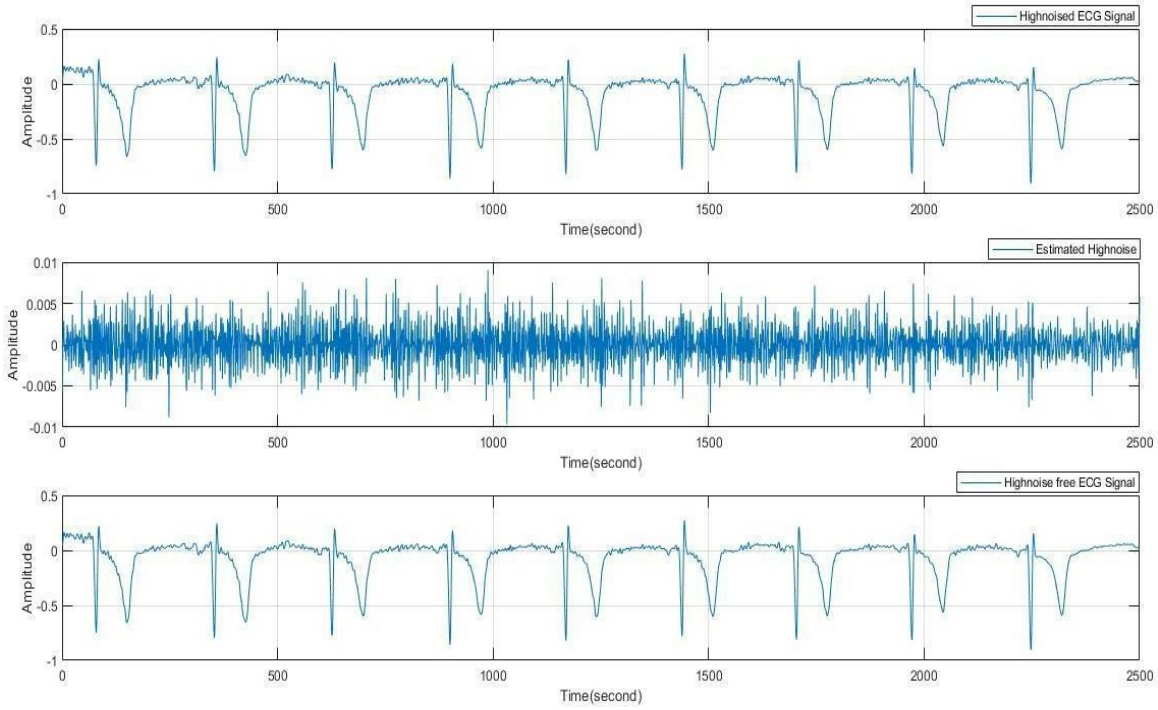

Figure 5.21 Elimination of High-frequency noise of EDB dataset in e0107 record

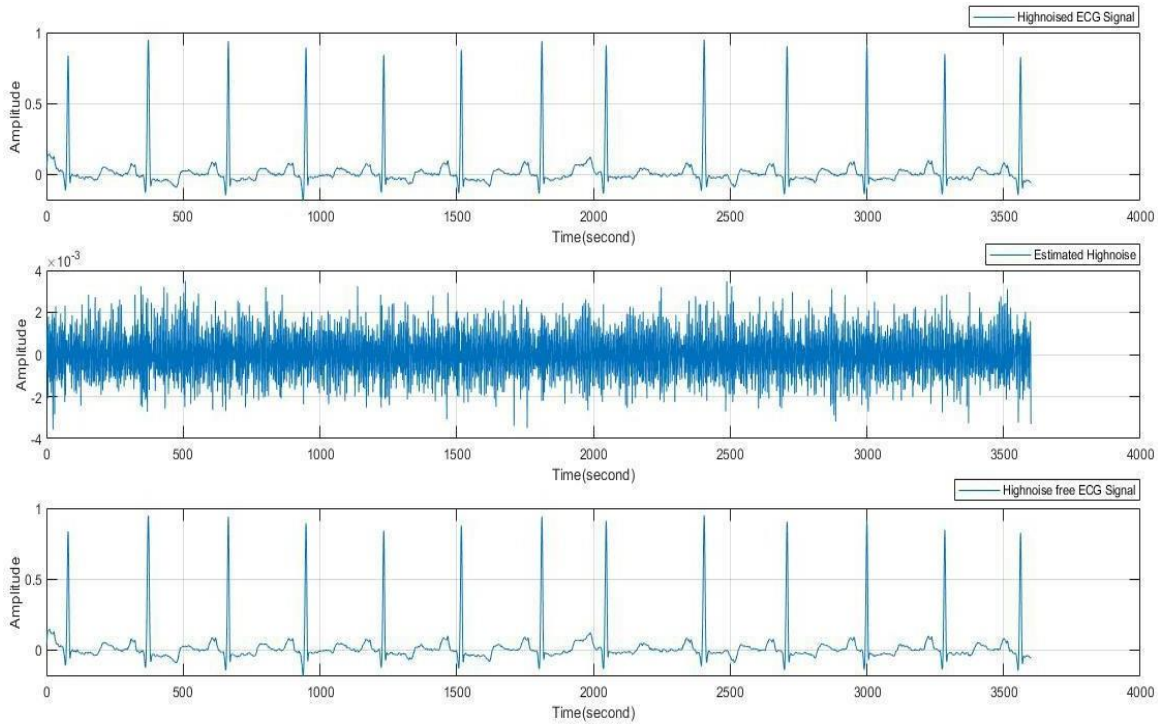

Figure 5.22 Elimination of High-frequency noise of MIT-BIH dataset in 100 records

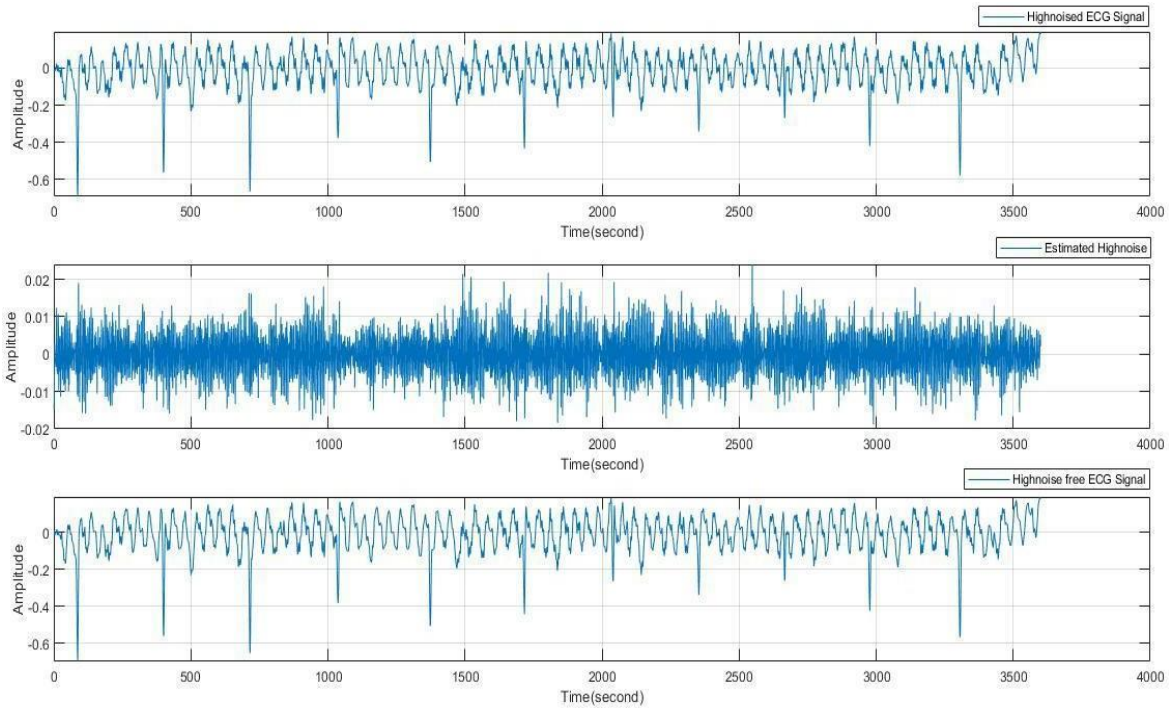

Figure 5.23 Elimination of High-frequency noise of MIT-BIH dataset in 101 record

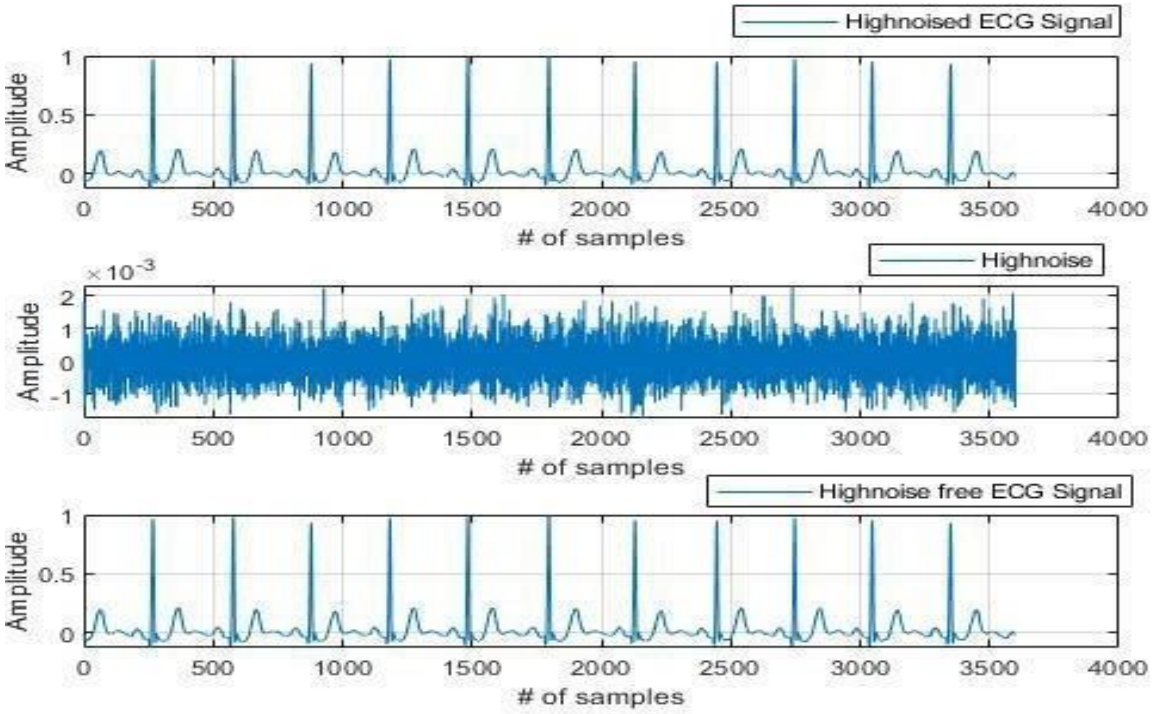

Figure 5.24 Elimination of High frequency noise of MIT-BIH dataset in 103 record

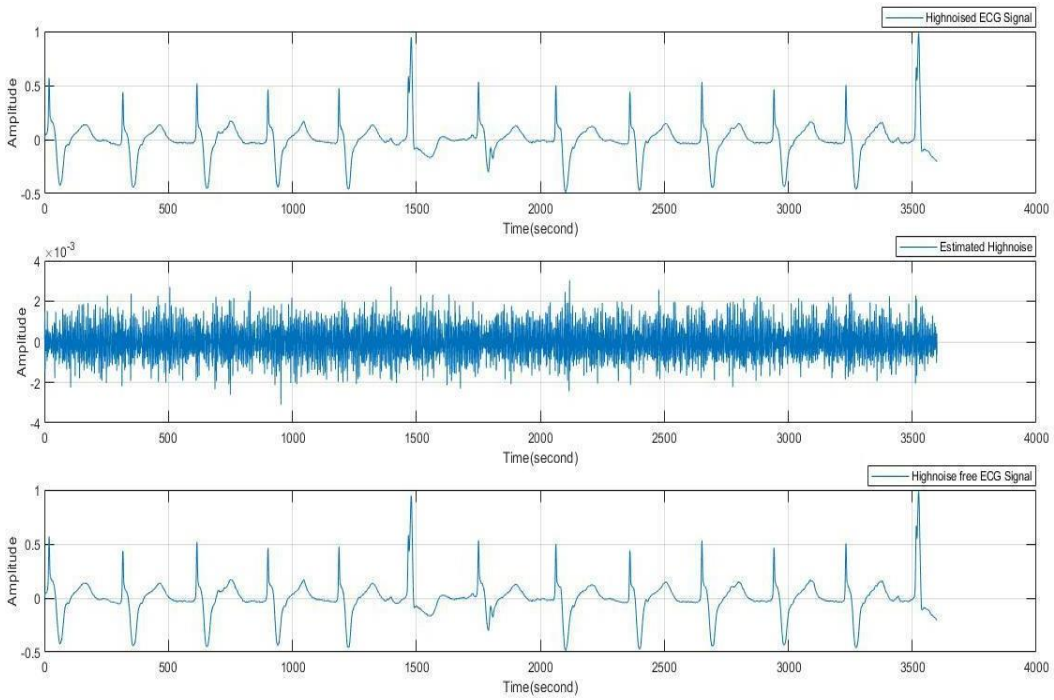

Figure 5.25 Elimination of High-frequency noise of MIT-BIH dataset in 104 record

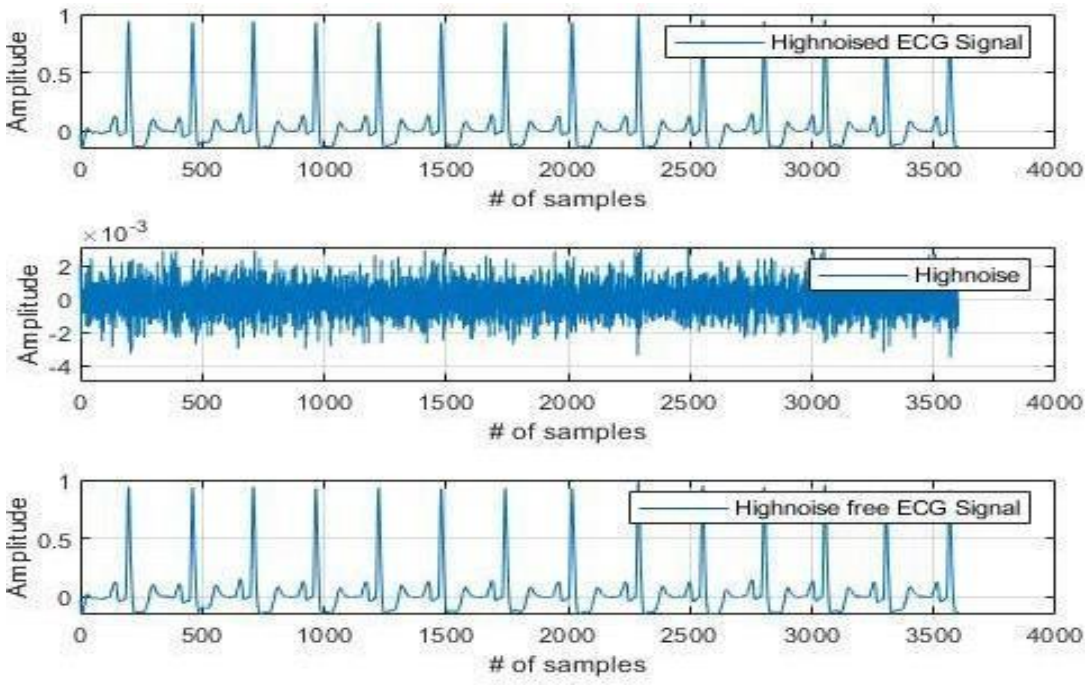

Figure 5.26 Elimination of High-frequency noise of MIT-BIH dataset in 105 record

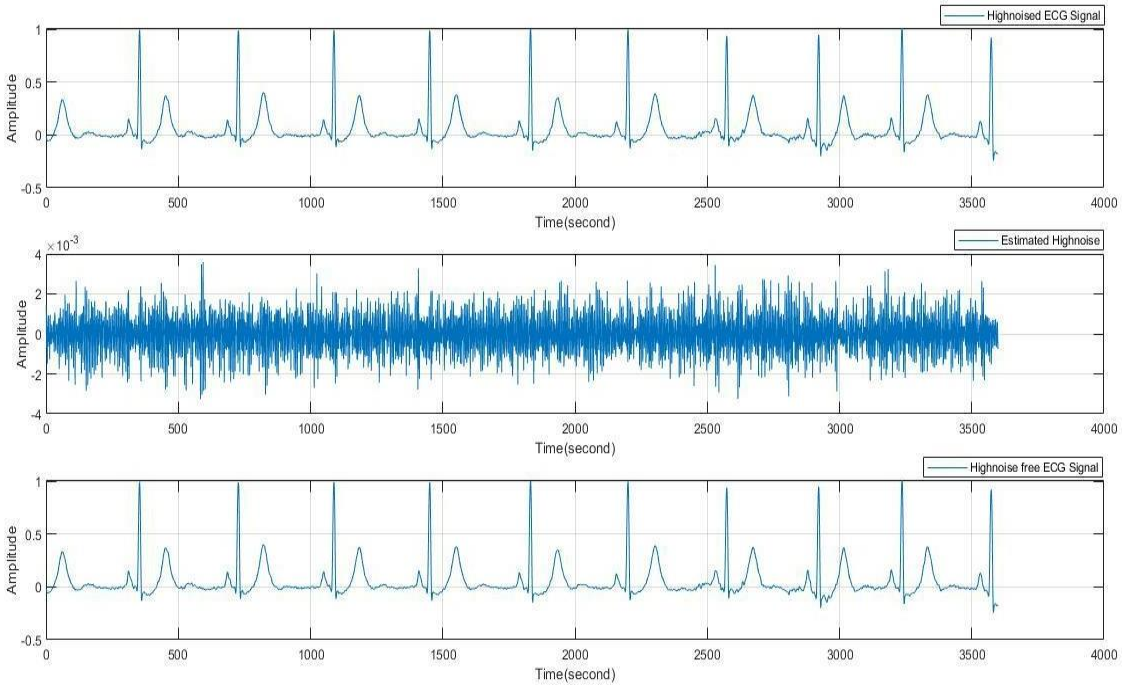

Figure 5.27 Elimination of High-frequency noise of MIT-BIH dataset in 106 record

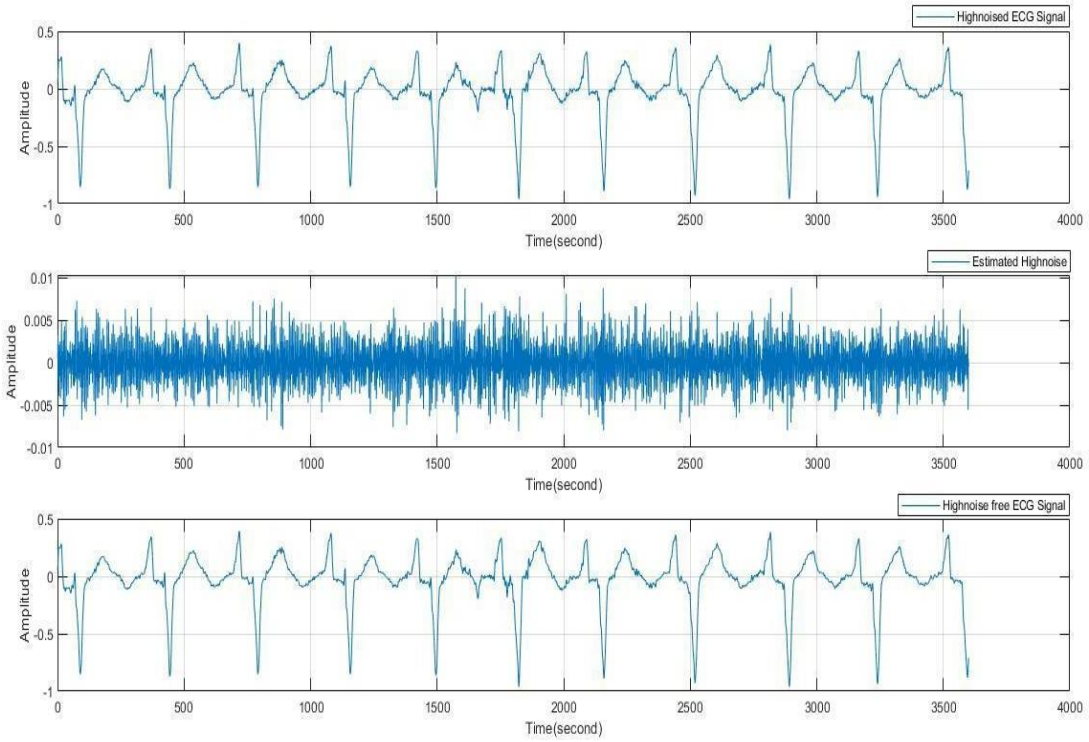

Figure 5.28 Elimination of High-frequency noise of MIT-BIH dataset in 108 record

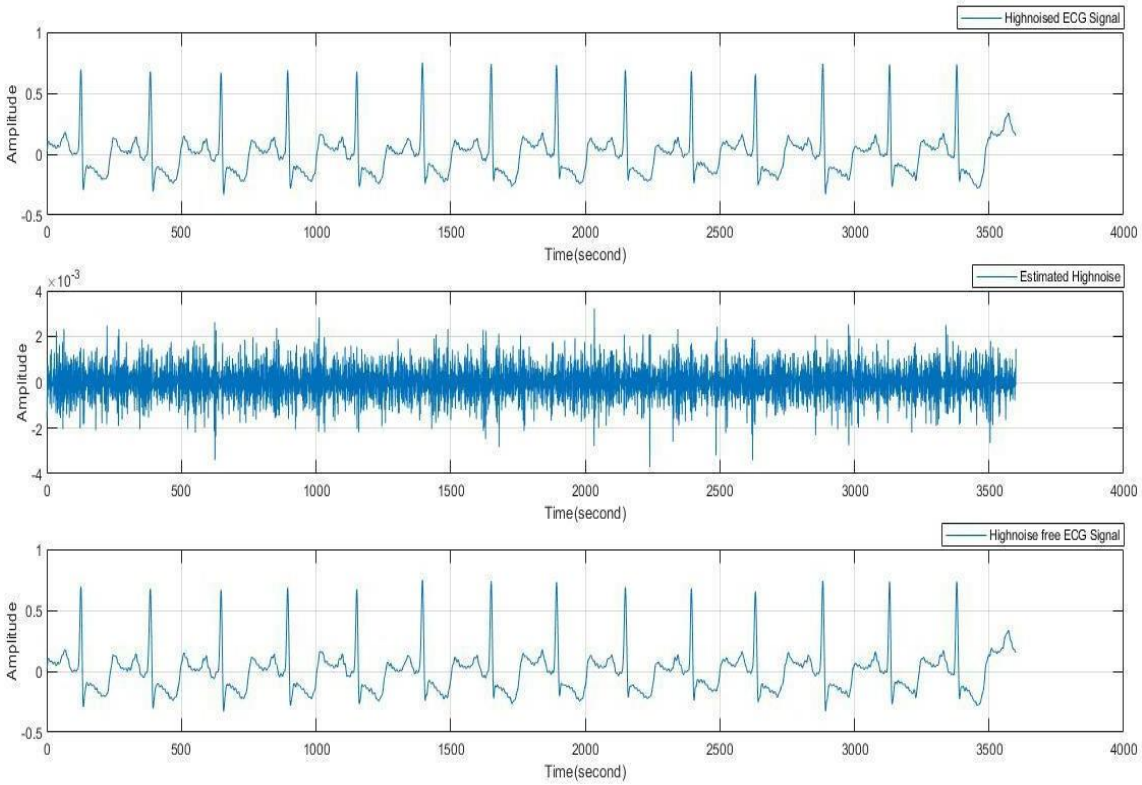

Figure 5.29 Elimination of High-frequency noise of MIT-BIH dataset in 112 record

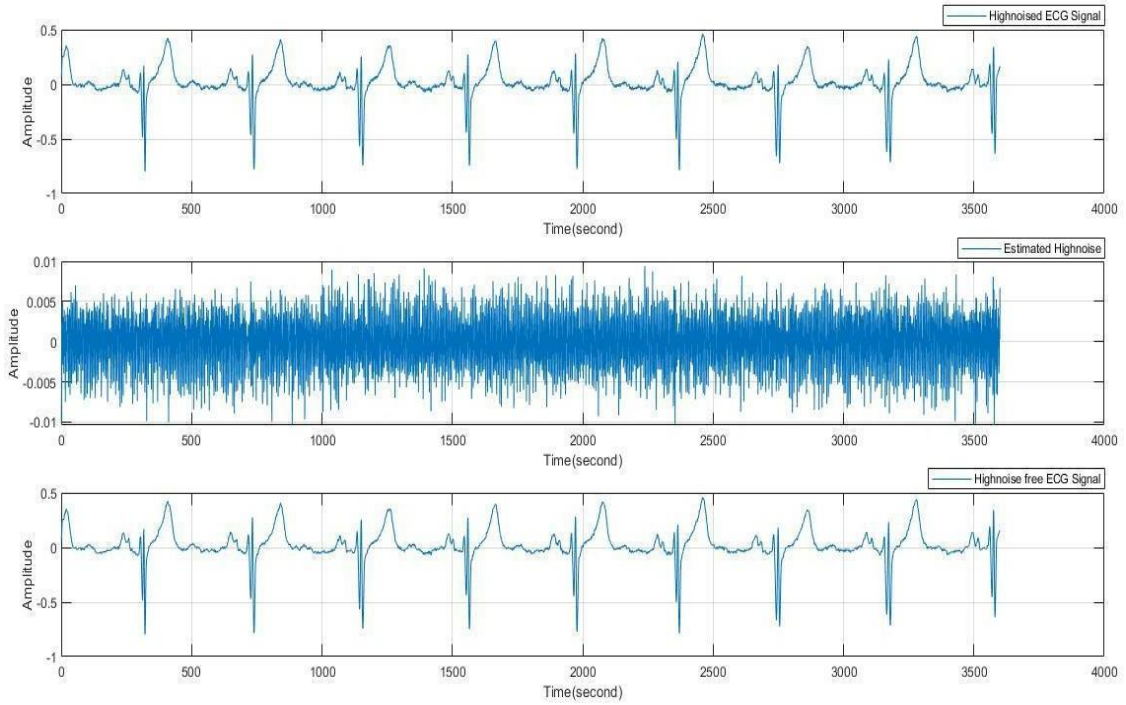

Figure 5.30 Elimination of High-frequency noise of MIT-BIH dataset in 114 record

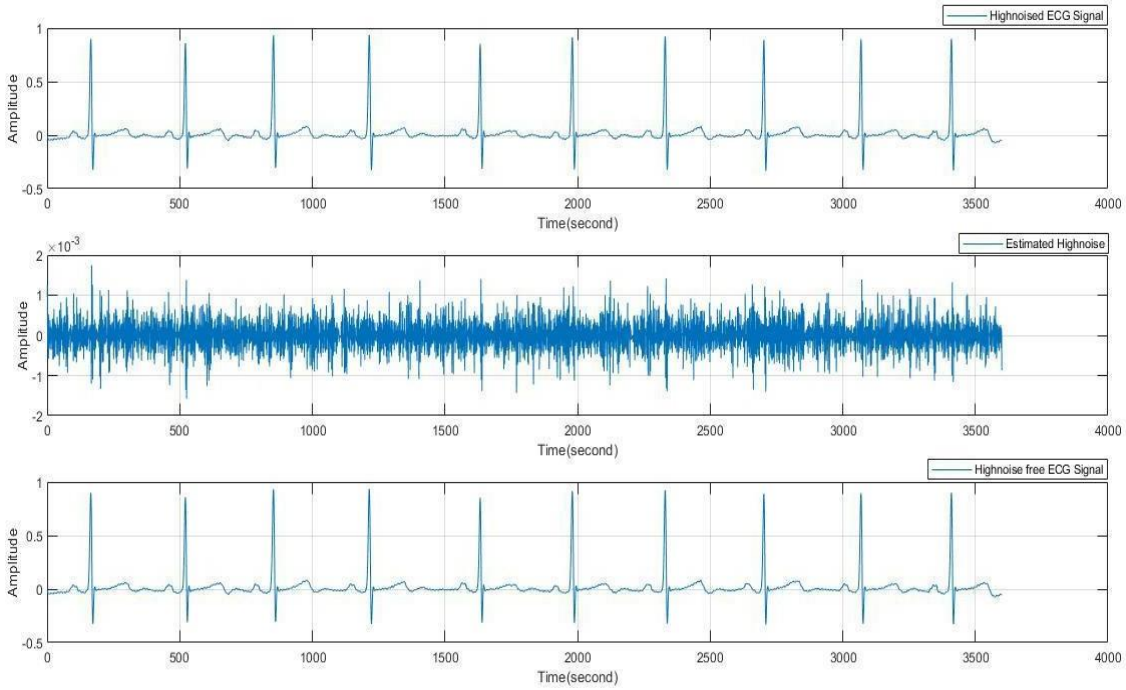

Figure 5.31 Elimination of High-frequency noise of MIT-BIH dataset in 115 record

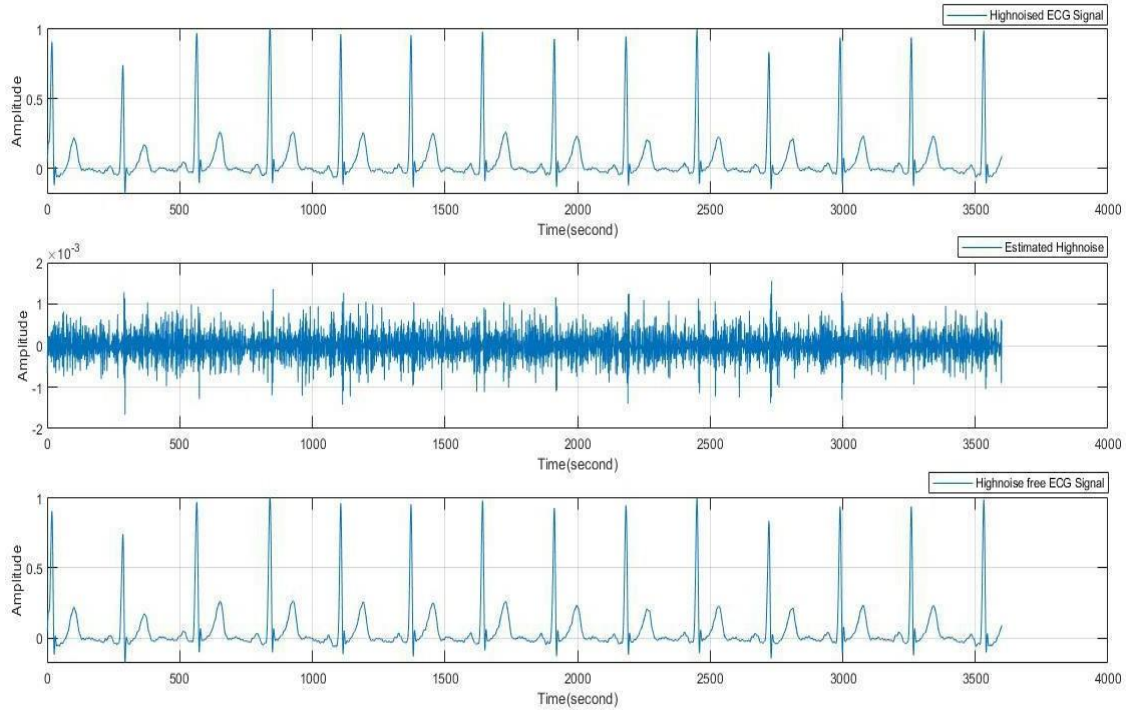

Figure 5.32 Elimination of High-frequency noise of MIT-BIH dataset in 116 record

5.3 Compared with Existing Approaches

Various techniques for removing baseline wandering and high-frequency noise are analyzed and examined in the introduction section. In [A.K. Sangaiah et al., 2019], the wavelet transform approach is used for the MIT-BIH database, which contains an IIR filter for noise reduction, and signal-to-noise ratio (SNR) is derived. In [A.K. Manocha and M. Singh, 2015], a wavelet–based technique is used for denoising in a European ST-T database. The percentage to per cent root-mean-square difference (PRD) is calculated after using different wavelet families. This proposed work compares Signal to noise ratio and Mean square error with various datasets [A.K. Sangaiah et al., 2019; D. Zhang et al., 2019]. The Signal Noise ratio, or MSE, for these datasets is determined here, and the results we have calculated are better than the existing work, as given in Table 5.1 and Table 5.2.

Table 5.1. Comparison of SNR using different records of different database

Sr.no	**SNR(db)**				
	European ST-T Database	MIT-BIH Database	Wavelet transform with IIR filter for MIT-BIH database [A. Sangaiah et.al, 2019]	Wavelet transform +median filter+SG filter median filter for European ST-T database (Proposed)	Wavelet transform +median filter+SG filter median filter for MIT-BIH Database (Proposed)
1	e0103	100	-9.6034	27	26.13
2	e0104	101	-4.2652	25	8.589
3	e0105	102	-7.5858	30	27.01
4	e0106	103	-4.2652	24.85	29.68
5	e0107	104	-4.6572	21.898	28.53
6	e0108	105	-5.2787	27	29.53
7	e0110	106	-6.75	22.2746	25.89

Table 5.2 Examination of the Mean square error using different records of different database

Sr. No.	MSE				
	European ST-T database	MIT-BIH Database	Wavelet transform with sub- band smoothing filter for MIT-BIH Database [D. Zhang et.al, 2019]	Wavelet transforms +median filter+SG filter median filter for European ST-T database (Proposed)	Wavelet transforms +median filter+SG filter median filter for MIT-BIH Database (Proposed)
1	e0103	100	0.00015	4.7387 e-06	8.9094 e-06
2	e0104	101	0.00018	6.0501 e-05	1.9905 e-06
3	e0105	102	0.00014	2.6055 e-06	1.041 e-06
4	e0106	103	0.00019	1.3532 e-05	5.1858 e-06
5	e0107	104	0.00018	1.5417 e-05	7.6531 e-06

5.4 Detection of ECG Characteristic Points

We added 100 sample points (zeros) before and after the pre-processed one-minute ECG segments to look for distinctive points in the pre-processed ECG signal. Local maxima are scanned across the entire ECG segment. These maxima are saved in the $(max)_h$ array. ECG max is defined as the highest value in this collection. ECG mean is a variable that stores the average value of all sample points in the signal. ECG amp is defined as (ECG_{max} – ECG_{mean})/2. ECG_thresh = (ECG_{max}) *(ECG_{amp}) for identifying all R peaks is the threshold for detecting R waves. R peaks are defined as all ECG record peaks that are above this threshold level [A.K Manocha and M. Singh, 2015; S. Banerjee et al., 2012; C. Li et al., 1995]. R INDEX holds the time position and amplitude of each R peak. After successfully detecting R peaks, the search moves back and forth between maxima and minima for P, Q, T, and S peaks. The first step is to look for a local maximum in window [R INDEX-400ms: R INDEX-200ms], which represents the P peak.

In the same way, [R Index-200ms: R_INDEX-40ms] is used for a local minimum where it yields a Q peak, is used. The search for a local minimum in the window [R INDEX+20ms: R INDEX+100ms] for such an S peak and a local maximum in the window [R INDEX+200ms: R INDEX+400ms] for the T peak follows a similar approach. P_INDEX, Q_ INDEX, S_INDEX, and T_INDEX contain the appropriate

sample locations and amplitudes of the observed characteristic waves. " represents the P, QRS complex and T peaks for 10 typical records from the European ST-T database and MIT-BIH database, as shown in Figure 5.33…… 5.37. Tables 5.3, 5.4 and 5.5 show the identified sample time values corresponding to these peaks (location) for standard (e0103), elevated (e0103), and depressed (e0105) signals throughout 10 seconds.

5.4.1 Onset and Offset Points Detection

The search for the corresponding INDEX to verify the slope sign inversion is initiated within the window for the onset and offset points of each characteristic wave. As given in Eqn. (5.1), the slope is calculated using Newton's difference quotient expression. The onset window is [INDEX-80ms: INDEX] while the offset window is [INDEX: INDEX+80ms].

$$\frac{f(x+h)-f(x)}{h} \qquad (5.1)$$

The slope of a secant line passing through the points (x+h, f (x+h)) and (x, f (x)) was determined using a basic two-point estimator. 'h' represents one sample interval in this case. The start and offset points that result have nearly zero slopes. The ON and OFF indices are then used to hold equivalent onset and offset sample values. In Figure 5.33…… Figure 5.37, black and blue stars represent the onset and offset sample values, respectively [A.K. Manocha and M. Singh, 2015] [Z. Zidelmla et.al, 2012]. Table 5.3, Table 5.4 and Table 5.5 show the detected sample time value for onset and offset points for normal, elevated (e0103), and depressed (e0105) signals throughout a 10-second period.

5.4.2. Calculation of Heart Rate

The heart rate, expressed in beats per minute, is calculated by measuring the distance between the two corresponding R-R intervals (BPM). An ECG record represents the average amount of time spent between R and R. intervals in the 60 seconds. Table 5.3, Table 5.4 and Table 5.5 show the observed heart rate for normal (e0103), elevated (e0103), and depressed (e0105) signals throughout 10 seconds.

5.4.3 Isoelectric Reference Detection (IR)

The TP segment determines the isoelectric reference, which is the region between the current beat's offset and the next beat's onset. This segment is a flat line between these

two places, and the voltage in this segment is essentially nil. The average isoelectric reference value for all beats is calculated for each record. Table 5.3, Table 5.4 and Table 5.5 show the observed isoelectric reference for normal and elevated for the record (e0103) and depressed signal for the record (e0105) throughout 10 seconds.

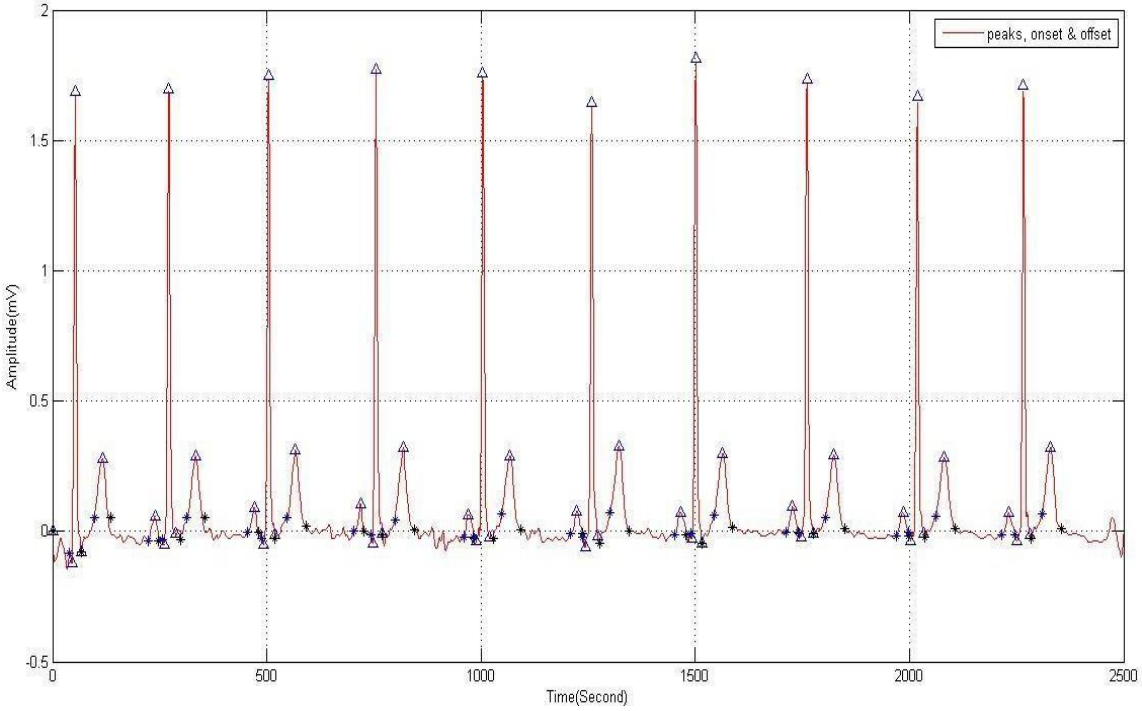

Figure 5.33 Delineation results for e0103 record

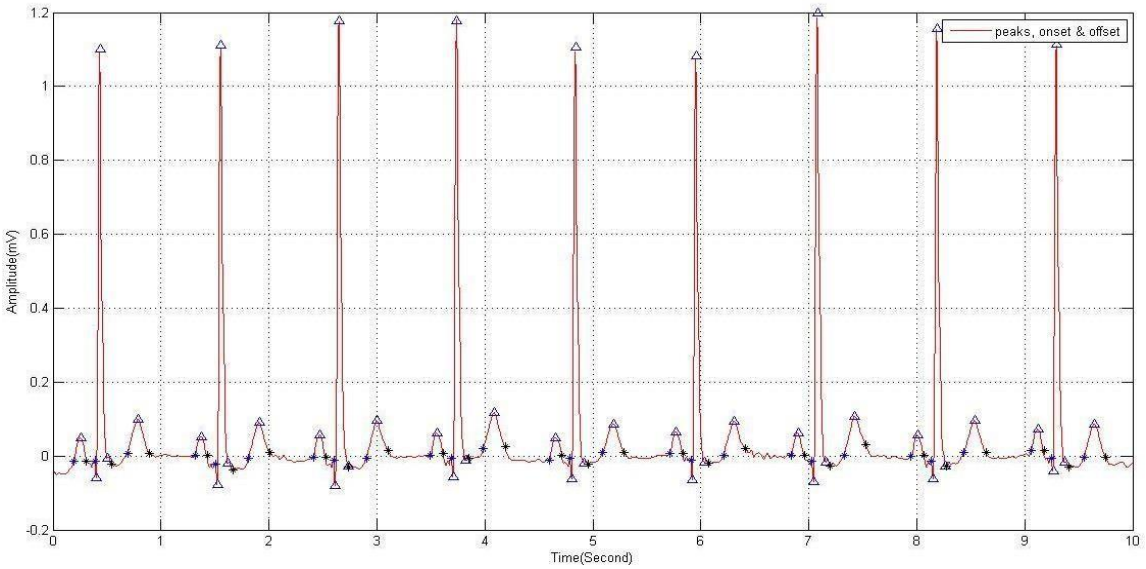

Figure 5.34 Delineation results for e0105 record

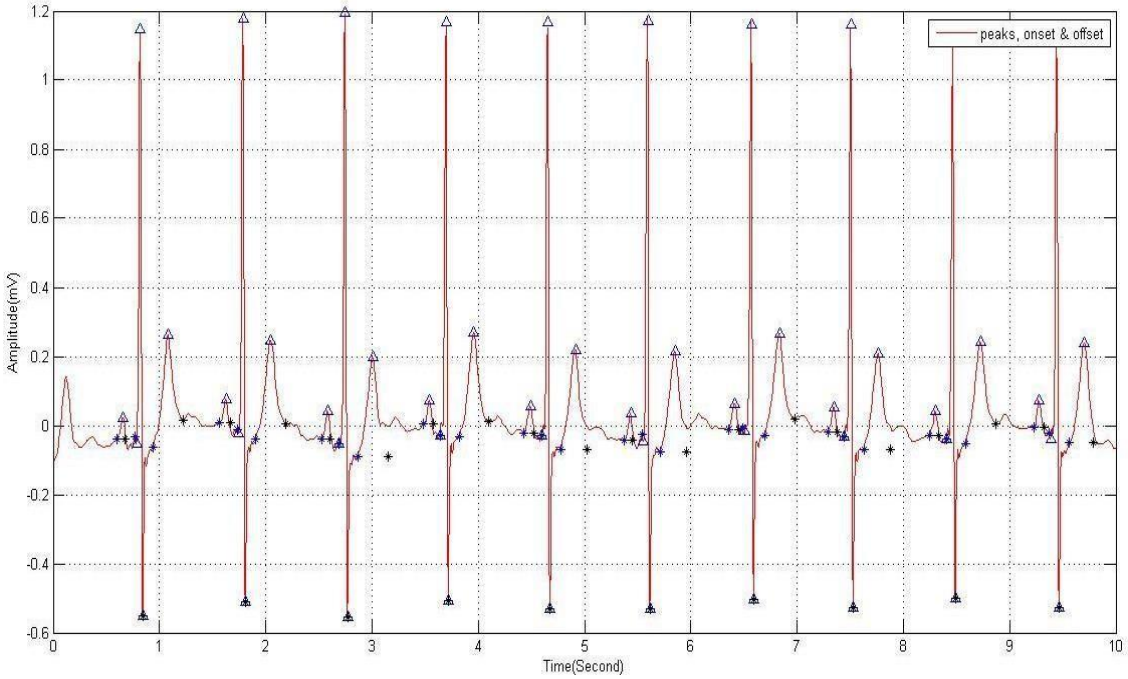

Figure 5.35 Delineation results for e0113 record

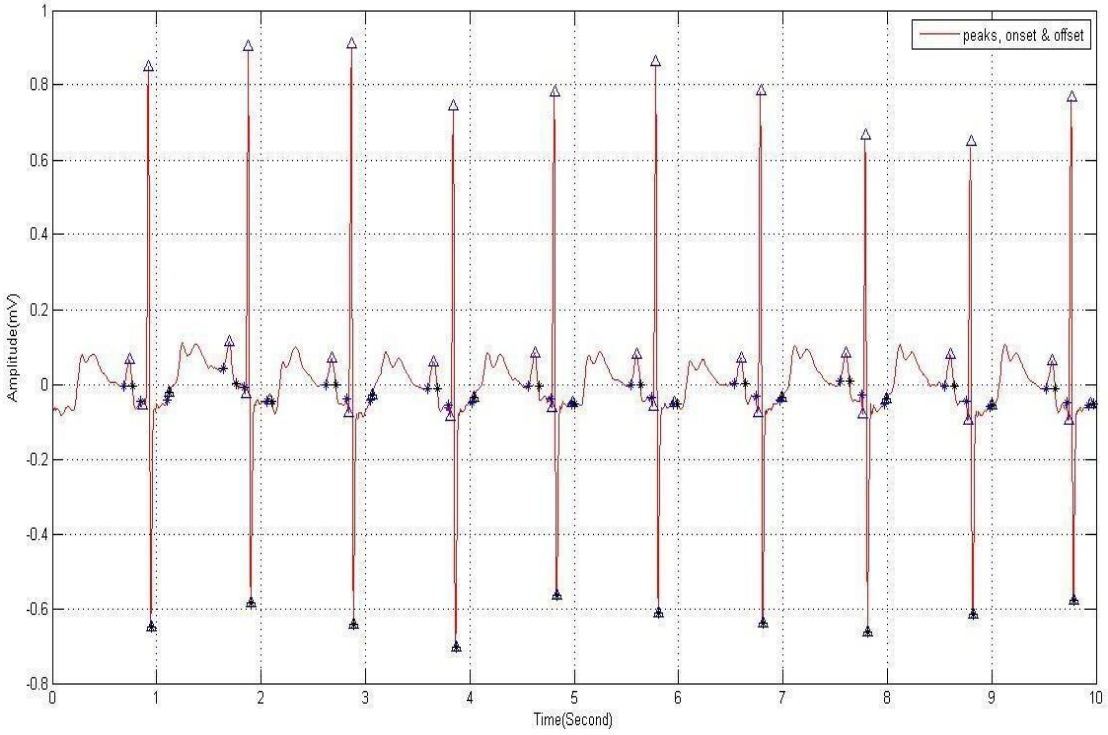

Figure 5.36 Delineation results for e0159 record

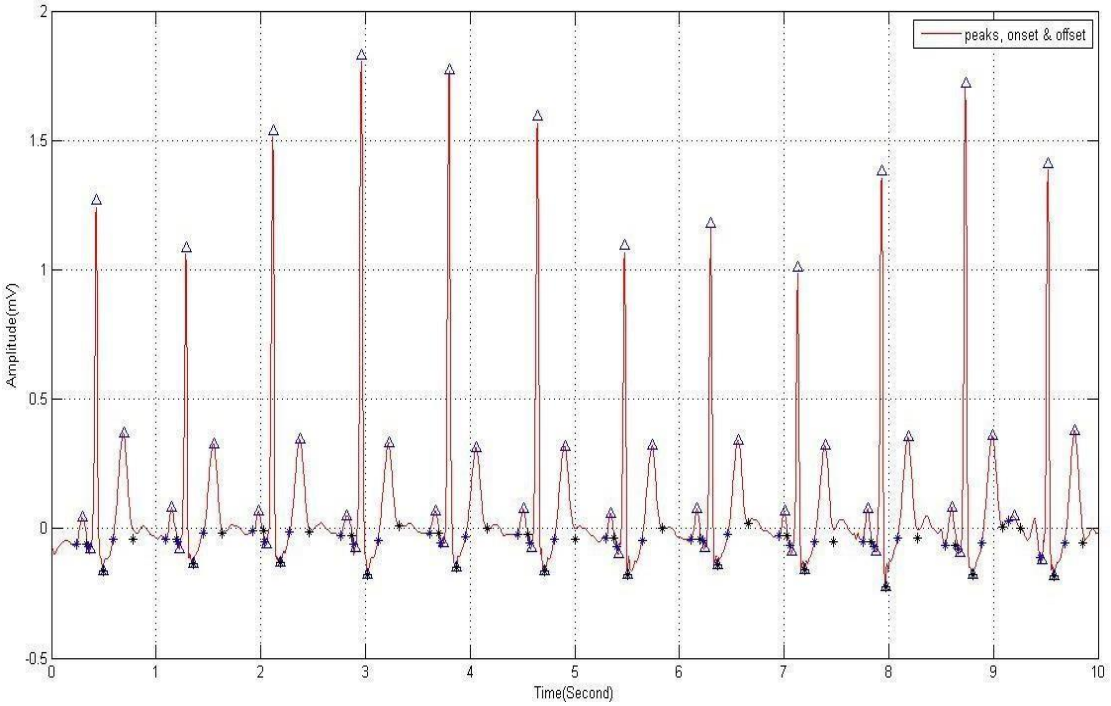

Figure 5.37 Delineation results for e0162 record

5.4.4 Identifying Amplitude Characteristics

The amplitude features obtained from diagnosis characteristic points are carefully considered.Q height = QRS onset amplitude – Q peak amplitude

R height = R amplitude – isoelectric reference from TP region

S height = QRS offset amplitude -S amplitude

P height = P amplitude – isoelectric reference from TP region

T height = T peak amplitude – isoelectric reference from TP region

5.4.5 Identifying Time Plane Characteristics

The time-plane characteristics obtained from detecting the onset and offset points of characteristicwaves are as follows:

R–R interval = Distance between two consecutive R peaks

PR interval = P onset: R peak location

QRS width = QRS onset: QRS offset

ST interval= S onset: T offset

QT interval = QRS onset: T offset

The QT interval's normalized value is corrected (hypothetically at a rate of 60 beats per minute) as given by Eqn. (5.2)

$$QTc = \frac{QT\ Interval}{\sqrt{R-R\ Interval}} \tag{5.2}$$

Table 5.3, Table 5.4 and Table 5.5 demonstrate the amplitude and time plane feature for normal (e0103), elevated (e0103), and depressed (e0105) records of 10 seconds duration.

Table 5.3 Amplitude and Time Plane Features for Delineated Characteristic Waves for Normal Signal

ECG parameters (Amplitude -mV & Location/ Interval- Second)	**Calculated values of e0103 normal signal (10 sec duration) of European ST-TDatabase**									
P_height (mV)	0.08	0.086	0.100	0.110	0.0857	0.0999	0.0978	0.104	0.0792	0.08
Q_height (V)	0.03	0.018	0.023	0.0349	0.0063	0.0394	0.0199	0.0152	0.0303	0.026
R_height (V)	1.76	1.725	1.757	1.77	1.782	1.664	1.837	1.743	1.675	1.732
S_height(mV)	-0.02	- 0.02	-0.013	-0.0054	- 0.0049	-0.0295	-0.0019	-0.0025	-0.0140	-0.01
T_height(mV)	0.362	0.31	0.317	0.3278	0.3127	0.3467	0.3232	0.3016	0.2872	0.32
PLoc	0	0.95	1.884	2.876	3.88	4.896	5.864	6.908	7.94	8.92
QLoc	0.144	1.04	1.968	2.988	3.952	4.972	5.968	6.988	8.012	9.0
Rloc	0.204	1.08	2.012	3.012	4.012	5.028	6	7.036	8.068	9.06
SLoc	0.264	1.13	2.072	3.072	4.072	5.088	6.06	7.096	8.128	9.12
TLoc	0.468	1.33	2.268	3.276	4.272	5.284	6.256	7.292	8.324	9.31
ST segment	0.271	0.236	0.296	0.3	0.256	0.284	0.288	0.292	0.288	0.28
QRS width(sec)	0.108	0.17	0.132	0.116	0.188	0.156	0.112	0.14	0.152	0.15
QTinterval(sec)	0.402	0.40	0.424	0.412	0.44	0.436	0.396	0.428	0.436	0.43
QTc(sec)	-	0.433	0.438	0.411	0.441	0.429	0.404	0.406	0.43	0.44
PRinter(sec)	-	0.192	0.196	0.208	0.176	0.2	0.204	0.2	0.196	0.20
R-R interval(sec)	0.91	0.87	0.932	1.004	0.996	1.016	0.972	1.04	1.028	0.99
Heart Rate(bpm)	68									

Table 5.4 Elevated Signal of Record e0103 of 10 (second) duration of European ST-T Database

ECG parameters(Amplitude -mV & Location/ Interval- Second)	Calculated values of e0103 elevated signal of 10 second duration of European ST-TDatabase									
P_height (mV)	0.073	0.097	0.096	0.109	0.095	0.114	0.103	0.098	0.088	0.09
Q_height (mV)	0.0014	0.0003	0.013	0.0003	0.0019	0.033	0.021	0.018	0.019	0.03
R_height (mV)	1.789	1.723	1.743	1.778	1.803	1.783	1.772	1.847	1.87	1.788
S_height (mV)	-0.0004	-0.0041	-0.0079	-0.0067	- 0.0193	-0.0058	-0.0024	-0.0177	- 0.00532	-0.00642
T_height (mV)	0.286	0.258	0.246	0.264	0.262	0.254	0.237	0.283	0.274	0.267
PLoc	0.292	1.288	2.236	3.212	4.168	5.152	6.14	7.072	8.02	8.988
QLoc	0.372	1.364	2.316	3.284	4.248	5.236	6.22	7.152	8.116	9.076
Rloc	0.432	1.424	2.376	3.344	4.308	5.296	6.276	7.212	8.156	9.12
SLoc	0.492	1.484	2.432	3.404	4.368	5.356	6.336	7.272	8.204	9.18
TLoc	0.68	1.676	2.628	3.588	4.56	5.548	6.524	7.456	8.404	9.368
ST segment	0.26	0.268	0.264	0.26	0.252	0.236	0.248	0.264	0.296	0.236
QRS width(sec)	0.144	0.148	0.164	0.148	0.136	0.192	0.156	0.132	0.108	0.156
QTinterval (sec)	0.402	0.404	0.424	0.412	0.44	0.436	0.396	0.428	0.436	0.436
QTc(sec)	-	0.433	0.438	0.411	0.441	0.429	0.404	0.406	0.43	0.44
PRinter(sec)	0.2	0.2	0.196	0.196	0.204	0.208	0.2	0.204	0.2	0.196
R-R interval (sec)	0.91	0.872	0.932	1.004	0.996	1.016	0.972	1.04	1.028	0.992
Heart rate (bpm)	62									

Table 5.5: Amplitude and Time Plane Features for Delineated Characteristic Waves for Depressed Signal

ECG parameters (Amplitude -mV & Location/ Interval- Second)	Calculated values of e0105 depressed signal of 10 second duration ofEuropean ST-T Database								
P_height(mV)	0.082	0.088	0.086	0.082	0.084	0.078	0.085	0.082	0.0829
Q_height(mV)	0.061	0.031	0.042	0.063	0.045	0.04	0.055	0.057	0.017
R_height(mV)	1.39	1.42	1.35	1.29	1.37	1.38	1.36	1.31	1.39
S_height(mV)	-0.047	-0.025	-0.011	-0.039	-0.054	0.005	0.009	-0.061	-0.008
T_height(mV)	0.13	0.151	0.152	0.143	0.138	0.139	0.141	0.141	0.124
PLoc	0.36	1.456	2.544	3.644	4.712	5.788	6.86	7.948	9.008
QLoc	0.504	1.596	2.692	3.784	4.856	5.932	7.012	8.088	9.152
Rloc	0.532	1.624	2.716	3.812	4.884	5.96	7.04	8.116	9.18
SLoc	0.592	1.684	2.776	3.872	4.944	6.02	7.1	8.176	9.24
TLoc	0.888	1.98	3.068	4.16	5.24	6.308	7.388	8.476	9.536
ST segment	0.344	0.392	0.396	0.312	0.32	0.388	0.392	0.324	0.344
QRS width(sec)	0.16	0.12	0.1	0.188	0.192	0.108	0.104	0.188	0.112
QTinterval(sec)	0.504	0.508	0.492	0.496	0.508	0.492	0.492	0.508	0.508
QTc(sec)	0.484	0.493	0.473	0.473	0.493	0.473	0.472	0.474	0.496
PRinter(sec)	0.236	0.232	0.236	0.232	0.236	0.236	0.244	0.232	0.236
R-R interval (sec)	1.087	1.092	1.092	1.096	1.072	1.076	1.08	1.076	1.064
Heart Rate(bpm)	56.01								

5.5 Effects of Artifact Removal on the Delineation Process

The artifacts, as previously mentioned, hurt the computerized ECG delineation. To avoid misdiagnosis, unnecessary testing, and therapeutic interventions, it is critical to recognize artifact frequencies and distinguish these artifact changes from genuine changes. Baseline wanders can affect ST segments in ECG signals, causing ST segment depression or elevation, which can be misinterpreted as myocardial ischemia.

High frequency can sometimes overlap with the QRS complex, creating the appearance of atrial flutter or fibrillation. P wave obliteration can resemble a heart block [S. Scheidt, 1984]. The discarding of wavelet coefficients corresponding to artifact frequencies of the original ECG signal has no adverse effects on the morphology of the original ECG signal, as illustrated in Figure 5.38, considerably

increasing the doctor's skill in defining the patient's appropriate treatment. Normal European ST-T Segment of the e0103m record from the European ST-T database was preferred to support the claim of improved ischemia detection sensitivity.

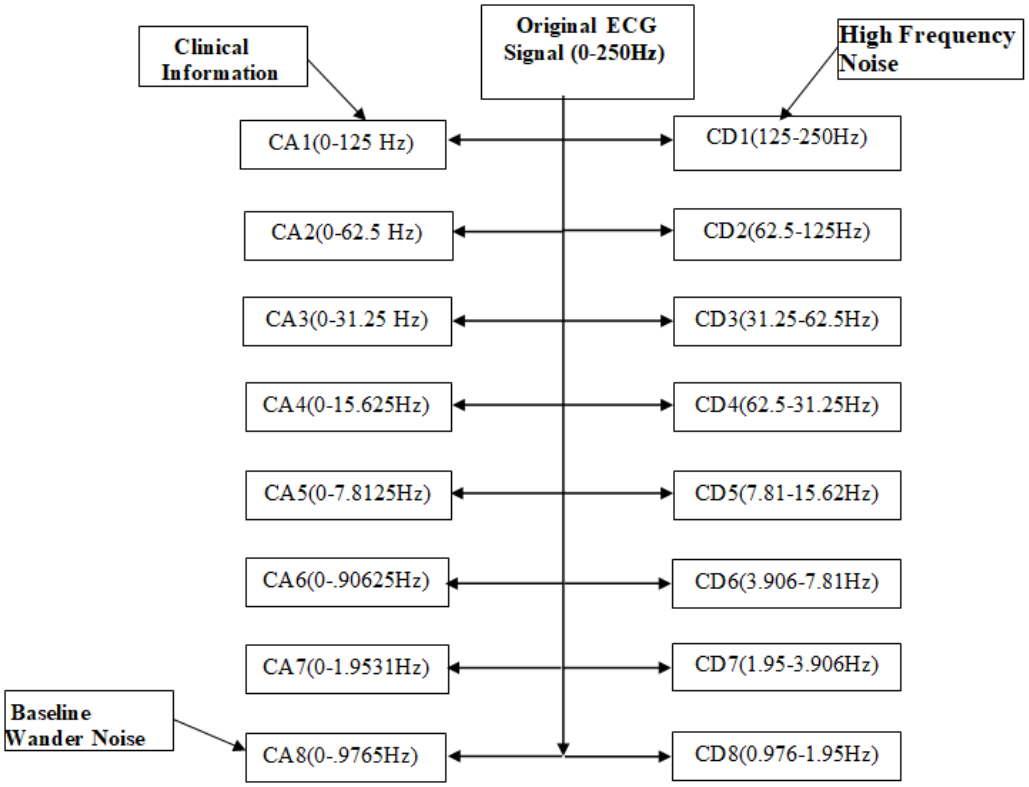

Figure 5.38 Frequency components of artifacts in wavelet decomposed ECG signals for European ST-T database

A 0.25 Hz baseline was superimposed to represent artifact due to breathing during the 1809 beats investigated. The remaining 623 beats were detected as ischemic, whereas 1186 beats were detected as normal. The normal signal's sensitivity drops to 65.56 percent due to false positives. When the proposed approach was used to remove this baseline wander, the sensitivity was restored to 100%. In computer-assisted ischemia detection, simply removing the baseline can increase sensitivity considerably.

In MATLAB 2018, the suggested approach for the delineation procedure is applied and evaluated for 10 typical ECG records of the European ST-T database (EDB) and all records of the MIT-BIH database and from Physio-bank. Furthermore, the peaks of all ECG characteristic points and their respective onset and offset sample values are manually validated against their original ECG data points in Microsoft Excel. The proposed technique was tested on 10 representatives during the entire recording as

well as the first hour of the e0103, e0104, e0105, e0108, e0113, e0114, e0147, e0159, e0162, and e0206 recordings.

These records provided a dataset of 43876 heartbeats for one recording lead. The final dataset contains 43,762 beats after removing artifacts and mis-detected beats during delineation. The proposed method is ineffective for detecting bi-phasic T waves (e0159 record), where T offset locations have been precisely identified. Table 5.6 demonstrates that for 10 typical records, omitting T waves of e0159 records, the average sensitivity is 99.94 %, and positive productivity is 99.98 %. The performance outcomes i.e., sensitivity (SE), and positive productivity (+P) were measured by employing Eqn. (5.3) and Eqn. (5.4) for above mentioned records.

$$\text{Sensitivity (SE)} = [TP/ (TP+FN)] *100 \quad (5.3)$$

$$\text{Positive productivity (+P)} = [TP/ (TP+FP)]*100 \quad (5.4)$$

Where TP is true positive, FP is false positive, and FN is false negative. The sensitivity and positive productivity measurements are defined in Eqns. (5.3) and (5.4). In addition to the above dataset, the developed delineation method has been validated on another dataset, which contains 37,333 for the first 30 minutes of e0103, e0104, e0105, e0108, e0113, e0114, and e0147, e0159, e0162, e0206. For this dataset, the developed technique, we have achieved 98.5 % average sensitivity and 98.3% average positive productivity, as given in Table 5.6.

Table 5.6 Evaluation Metrics for Ten Representative Recordings

Sr. No.	Record No.	No. of beats	S_E (%)	+P(%)
1	e0103	3696	99.98	99.87
2	e0104	7824	99.92	99.81
3	e0105	3357	99.81	99.84
4	e0108	3301	99.82	99.63
5	e0113	4225	99.38	99.67
6	e0114	2858	99.47	99.77
7	e0147	3261	99.64	99.69
8	e0159	4449	99.76	99.91
9	e0162	5294	99.78	99.86
10	e0206	5611	99.68	99.78
	Total	**43,876**	**98.5**	**98.3**

5.5.1 Comparisons with Existing Methods

Despite this, it is tough to compare the proposed method to existing methods due to the abundance of databases available in the literature for the validation process. QRS

detection methods are classified as syntactic, non-syntactic, and hybrid. Because of the need for grammatical inference, the syntactic approach [E. Pietka, 1991] is time-consuming. Non-syntactic methods preferred band pass filters, suppressing the P and T waves [Q. Xue, Y.H. Hu et al., 1992; P.S. Hamilton and W.J. Tompkins, 1986]. Most of the reported methods cannot detect the P wave following the detection of the QRS complex, which is commonly embedded in artifacts—the proposed method in [F. Gritzali, 1988] can detect P and T waves through length transformation but is not resistant to noise and artifacts. The pan- Tomkins method [J. Pan and W.J. Tomkins, 1985] used nonlinear transformations such as derivatives and squaring to detect the QRS complex of the ECG signal. Still, it has the following drawbacks: 1) Even within the same subject, the signal frequency band of the QRS complex varies between beats. 2) Artifact frequency bands and QRS complex frequency bands overlap. The proposed method preserves the small frequency waves of the P and T waves, as determined by Dhono's method [K. Daqrouq, 2005]. Table 5.7 compares the performance of the developed method to that of previously published methods for European ST-T database records. It should be noted that the comparative methods do not have the same number of datasets as the other methods. For ten representative ECG records, the developed delineation method achieves 99 percent sensitivity and 100 percent positive productivity. In comparison to other methods, the developed method has the highest positive productivity.

Table 5.7 Performance evaluation of developed method with existing method: application using European ST-T database

Detection Algorithm	SE (%)	+ P (%)
[J.P. Martinez et.al, 2004]	99.61	99.48
[G.B. Moody & R.G. Mark, 1982]	95.09	98.63
[A. Ghaffaria, 2009]	99.63	99.55
[L.Y.D. Macro and L. Chiari, 2011]	99.81	99.56
Proposed Method	**99**	**100**

5.6 Flow Diagram of R-peak detection using MIT-BIH Database

R-wave positions are defined as the de-noised ECG data's most significant amplitude. Figure 5.39 shows the flow chart for the detection of R-loc. To discover a satisfactory localization of the window of size 160 milliseconds around the QRS area, a practical threshold of 15% of the maximum amplitude of (D3+D4+D5) was carefully chosen.

A search procedure is started around the de-noised ECG beats to find amplitudes bigger than the predetermined threshold level. The signal's highest amplitude determines the R-peak placements in the chosen window. Between two successive searches in which ventricular depolarization cannot occur, therefore the period of 200 milliseconds is measured. The maximum peaks discovered are classified as R-peaks and are kept in an array of Rloc.

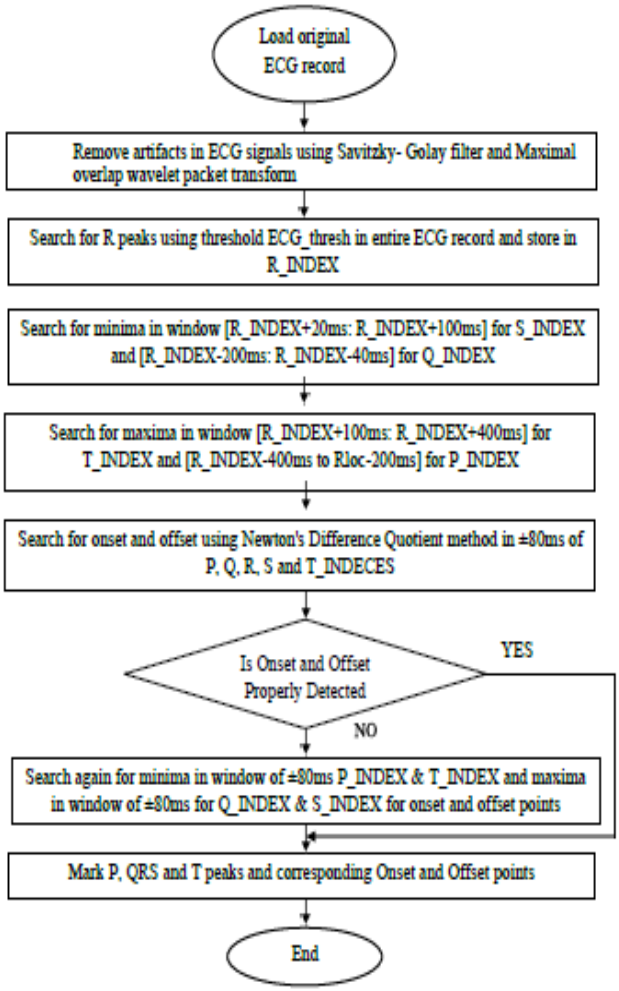

Figure 5.39 Flowchart for developed method for delineation process

5.6.1 Detection of QRS complex using MIT-BIH database

Based on their power spectrum of QRS band energy, the detail coefficients of DWT are selected to detect the QRS complex. Because of their physical resemblance to the QRS complexes, the three sets of detail coefficients D3, D4, and D5 are combined. By determining the fiducial position from the window's width (160 milliseconds), a sliding window of 200 milliseconds is utilized to detect the position of the R peak in

each window location.

5.7 Results for detection of characteristics point using MIT-BIH database

The MIT-BIH arrhythmia database assessed the proposed R-peak detection and QRS complex approach. The recorded ECG signals are satisfactory in terms of quality, waves, QRS components, and abnormal cardiac beats. Figure 5.42 to Figure 5.48 show the delineation results of ECG Signal (P, QRS, T peak detection) of MIT-BIH database for 103, 105, 106, 107, 108, 109, 111 record and Table 5.8 provides a summary of the results for all 48 records in the MIT-BIH arrhythmia database.

5.7.1 Detection of R-peak

Figures 5.40 to Figures 5.42 show an abnormal ECG signal that has been de-noised using Savitzky- Golay filter for baseline wander correction. The simulation findings for R Peak detection and QRS detection of 103 records of the MIT-BIH database are shown in Figures 5.41 and Figure 5.42.

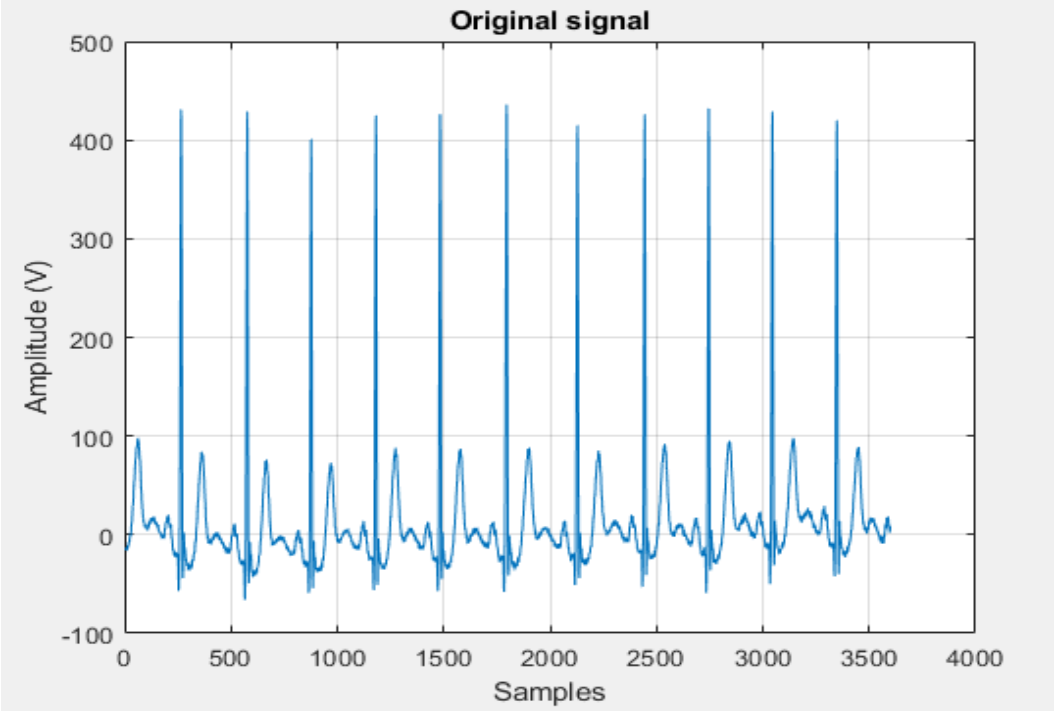

Figure 5.40 Original ECG signal of MIT-BIH database for record 103

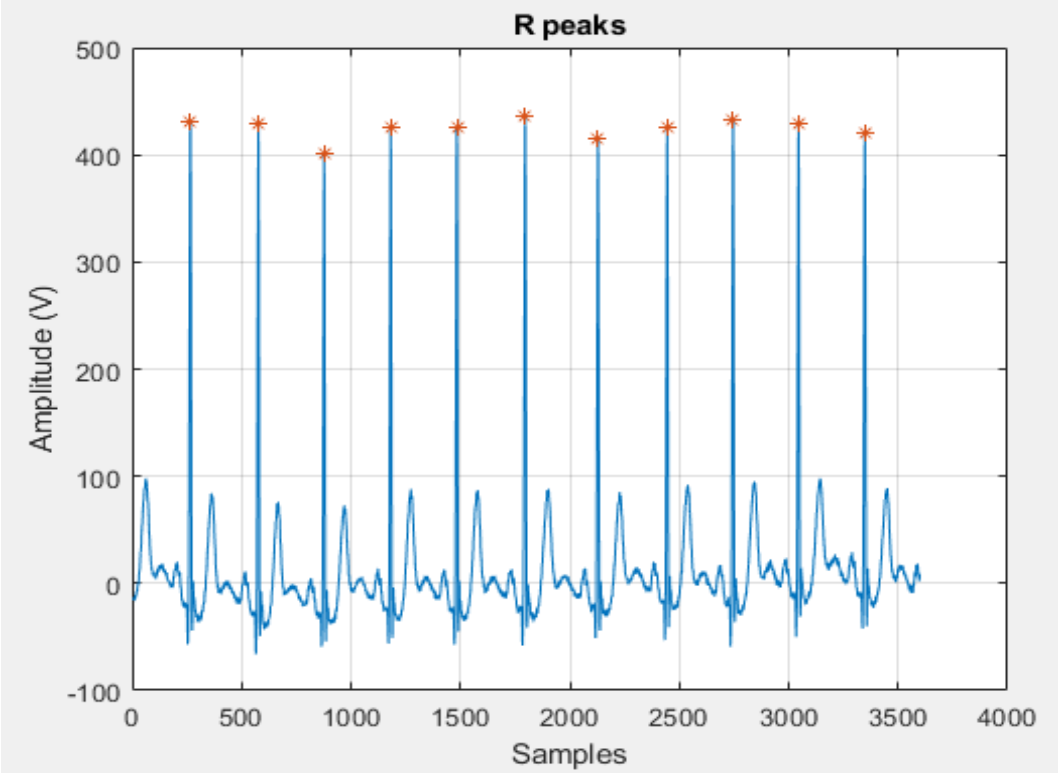

Figure 5.41 Detection of R Peak ECG signal of MIT-BIH database for record 103

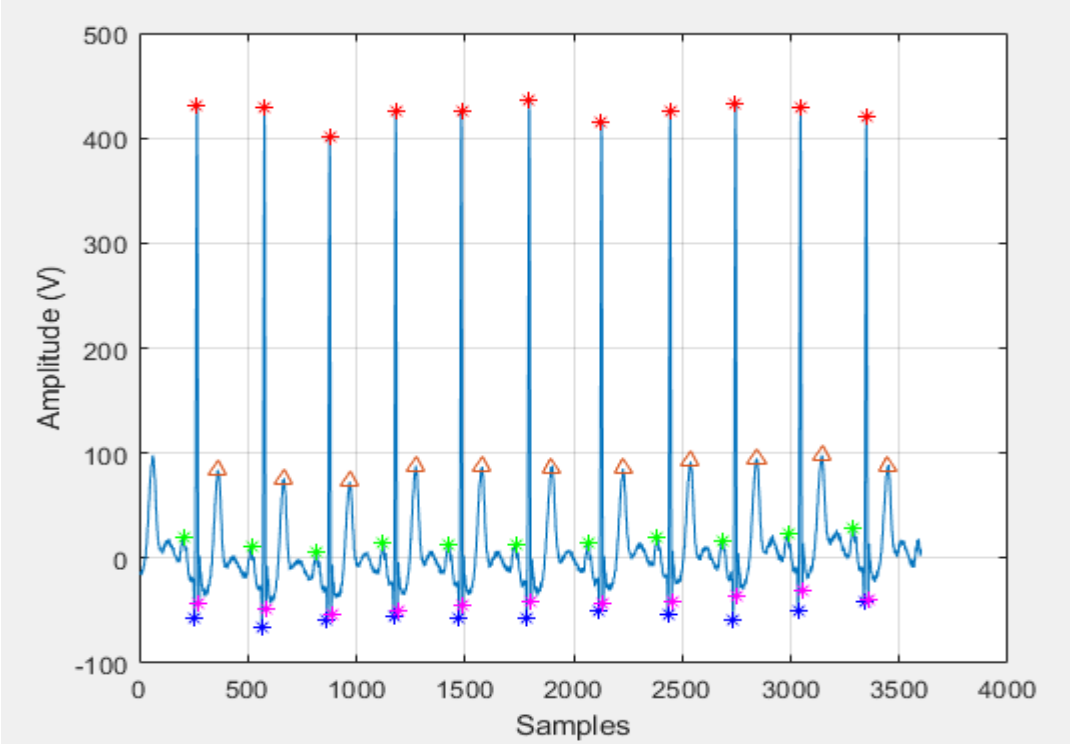

Figure 5.42 Delineation of ECG Signal (P, QRS, T peak detection) of MIT-BIH database for 103 record

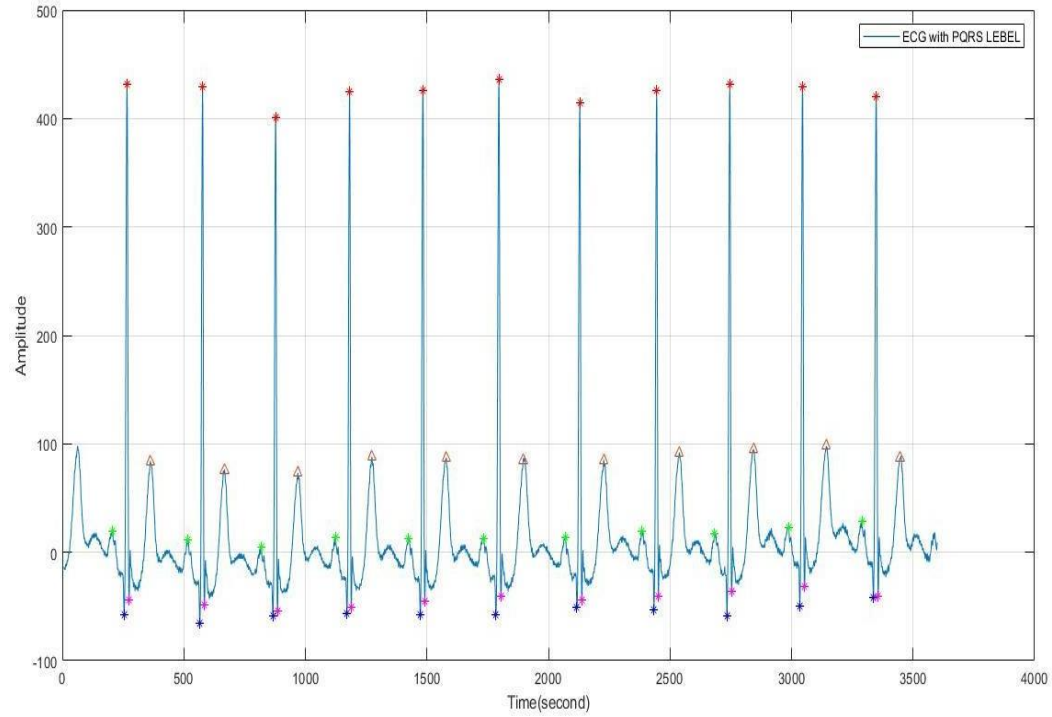

Figure 5.43 Delineation of ECG Signal (P, QRS, T peak detection) of MIT-BIH database for 105 record

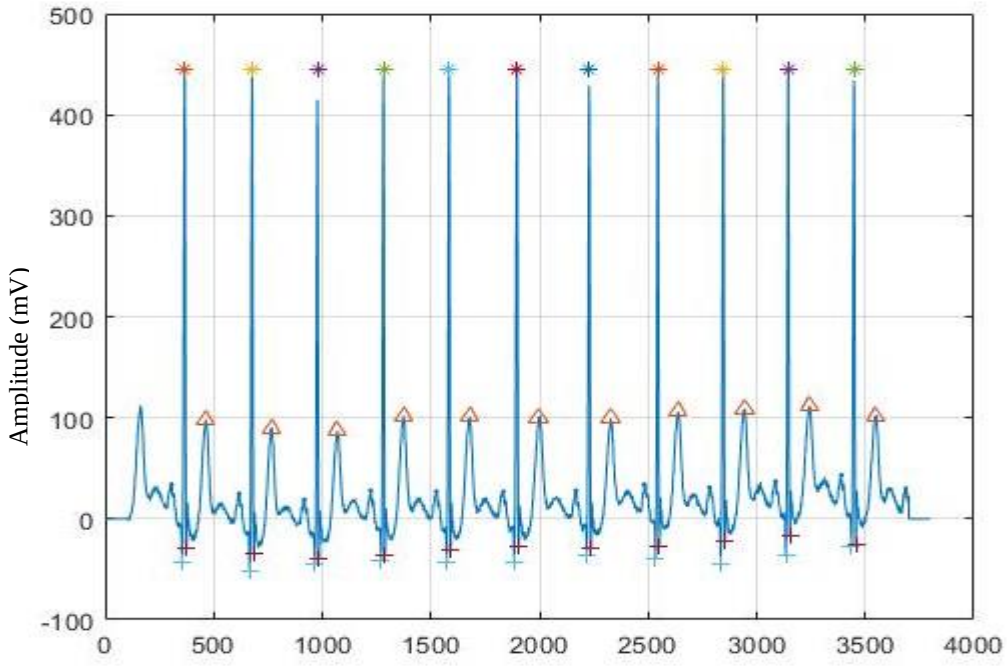

Figure 5.44 Delineation of ECG Signal (P, QRS, T peak detection) of MIT-BIH database for 106 records

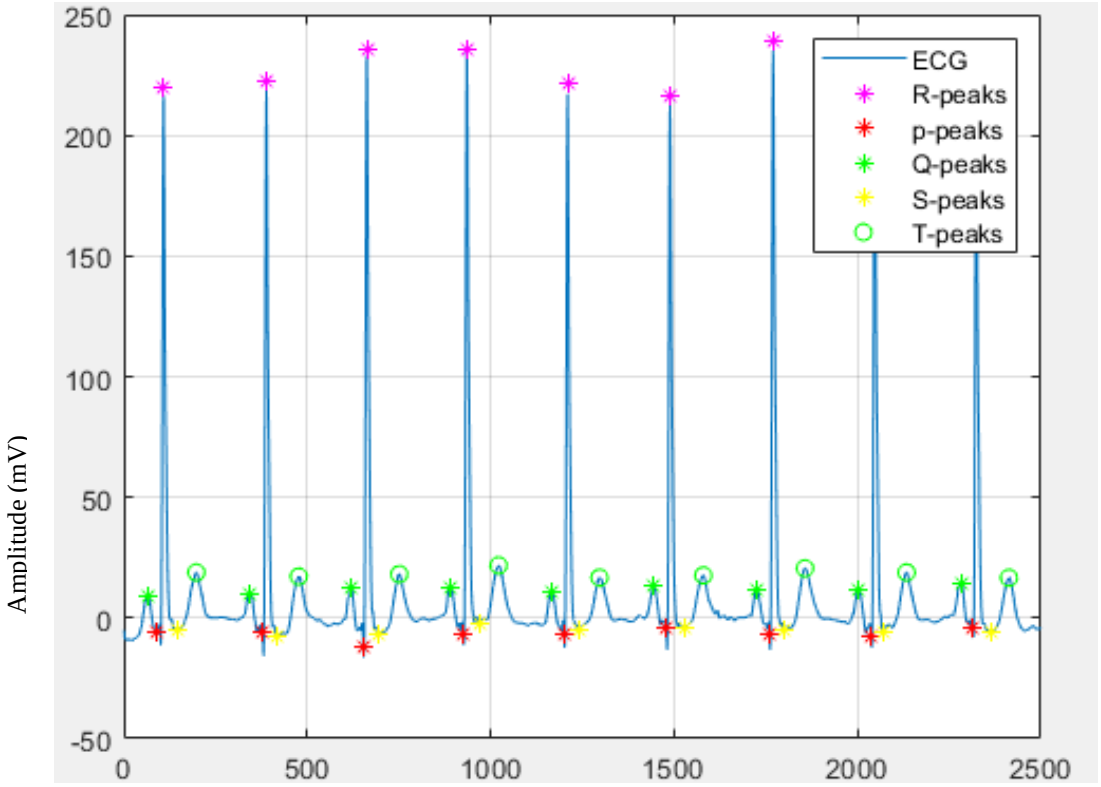

Figure 5.45 Delineation of ECG Signal (P, QRS, T peak detection) of MIT-BIH database for 107 record

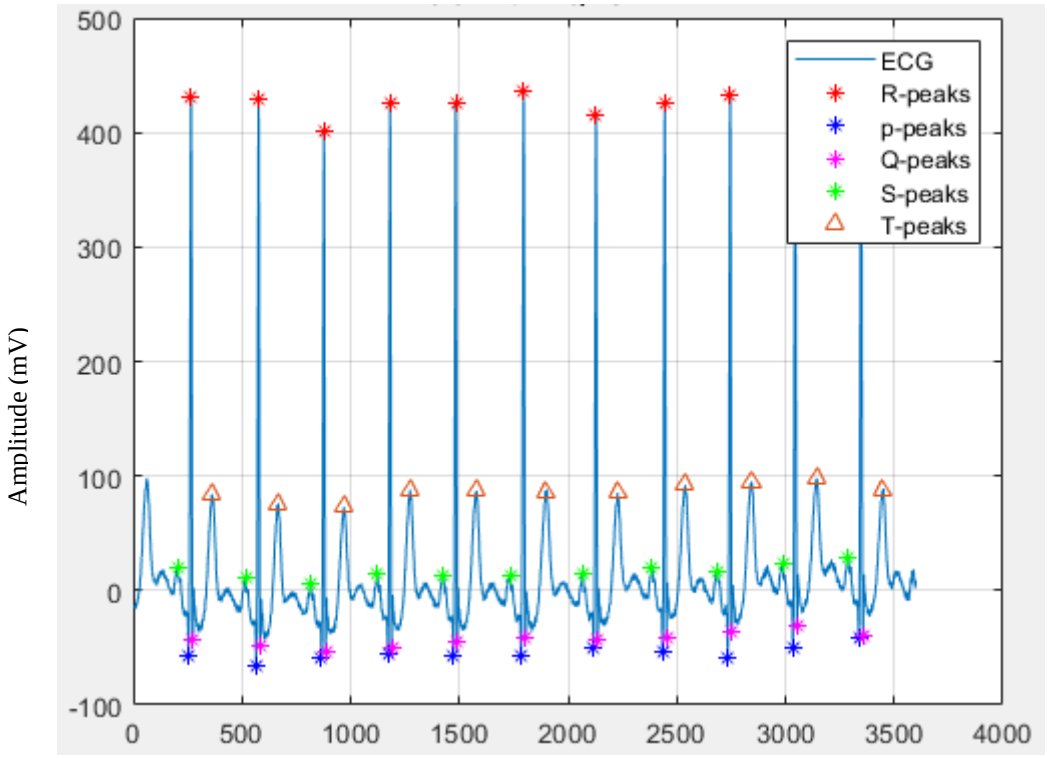

Figure 5.46 Delineation of ECG Signal (P, QRS, T peak detection) of MIT-BIH database for 108 record

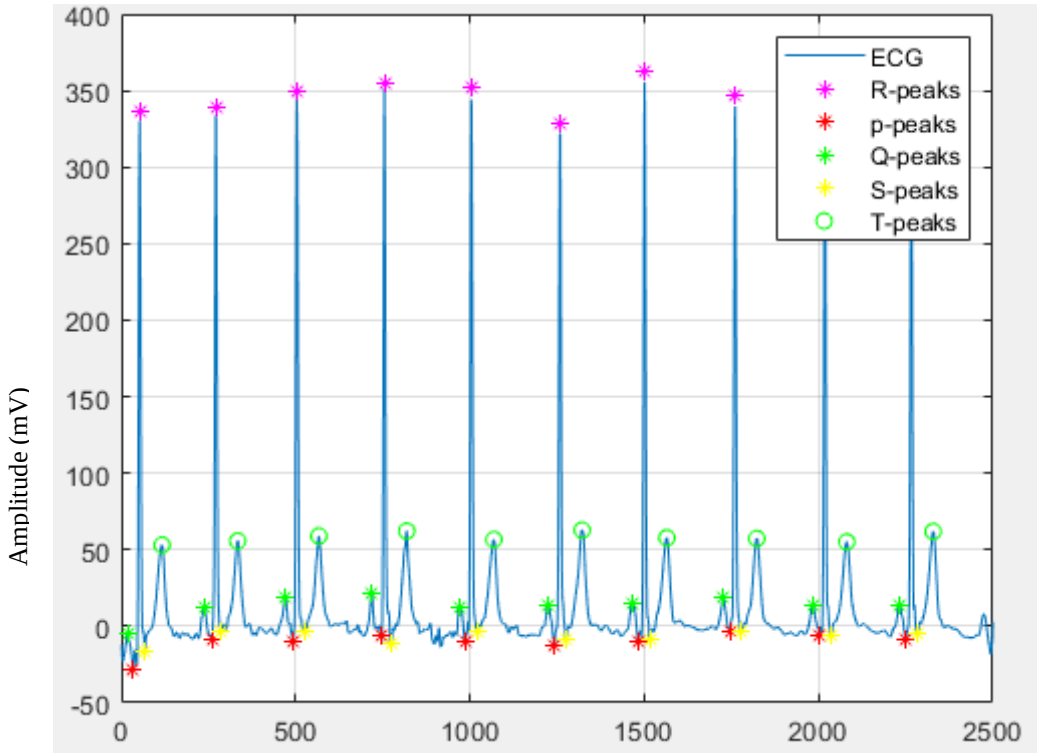

Figure 5.47 Delineation of ECG Signal (P, QRS, T peak detection) of MIT-BIH database for 109 record

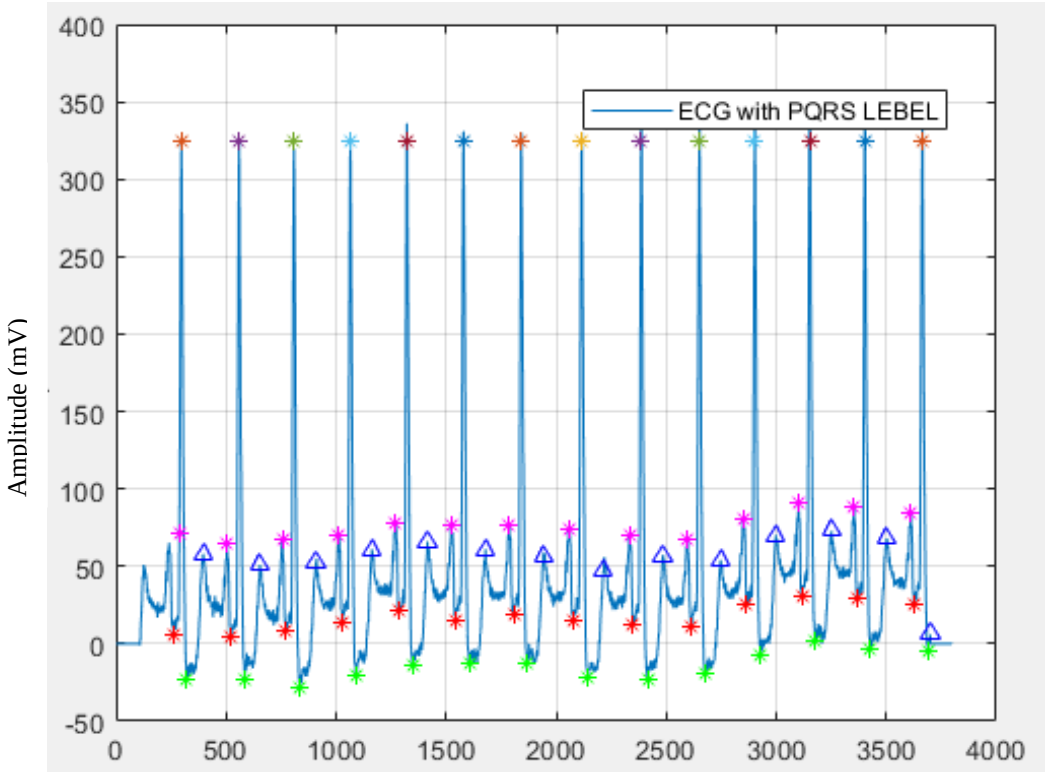

Figure 5.48 Delineation of ECG Signal (P, QRS, T peak detection) of MIT-BIH database for 111 records

Table 5.8 Extracted features of ECG recorded signals

Record#	Q_{amp}	R_{amp}	S_{amp}	T_{amp}	QT_Int	ST_Int	RR_Int	QRS_Dur
100	-0.156	0.792	-0.151	0.025	0.389	0.464	0.813	0.105
101	-0.089	0.809	-0.094	0.096	0.324	0.334	0.845	0.176
102	-0.084	0.785	-0.192	0.115	0.355	0.363	0.826	0.165
103	-0.149	0.926	-0.161	0.157	0.299	0.351	0.855	0.089
104	-0.027	0.434	-0.180	0.103	0.411	0.437	0.801	0.130
105	-0.041	0.703	-0.133	0.065	0.322	0.327	0.723	0.168
106	-0.082	0.748	-0.152	0.152	0.311	0.345	0.886	0.165
107	-0.066	0.616	-0.669	0.367	0.381	0.366	0.850	0.222
108	-0.028	0.303	-0.069	0.061	0.415	0.395	0.662	0.167
109	-0.069	0.726	-0.3567	0.117	0.411	0.406	0.655	0.183
111	0.024	0.739	-0.294	0.257	0.311	0.329	0.849	0.145
112	-0.019	0.822	-0.305	0.153	0.382	0.422	0.701	0.156
113	-0.101	0.891	-0.205	0.381	0.357	0.434	1.016	0.118
114	-0.576	0.219	-0.704	0.363	0.291	0.368	0.985	0.120
115	-0.047	0.903	-0.378	0.063	0.395	0.430	0.959	0.107
116	-0.088	0.908	-0.181	0.157	0.283	0.313	0.761	0.144
117	-0.122	0.655	-0.784	0.562	0.347	0.397	1.202	0.170
118	-0.016	0.773	-0.623	0.076	0.398	0.395	0.828	0.176
119	0.003	0.637	-0.113	0.081	0.342	0.364	0.830	0.118
121	-0.041	0.789	-0.021	0.115	0.309	0.325	0.999	0.206
122	-0.192	0.9201	-0.127	-0.013	0.309	0.333	0.687	0.198
123	-0.045	0.866	-0.348	0.168	0.373	0.415	1.252	0.118
124	-0.041	0.896	-0.121	0.026	0.421	0.432	1.210	0.125
200	-0.028	0.399	-0.399	0.165	0.355	0.389	0.682	0.147
201	-0.041	0.866	-0.094	0.121	0.311	0.292	0.667	0.170
202	-0.001	0.838	-0.058	0.178	0.331	0.314	1.125	0.191
203	-0.044	0.622	-0.206	0.202	0.357	0.327	0.572	0.186
205	-0.119	0.899	-0.099	0.062	0.325	0.382	0.669	0.110
207	-0.072	0.227	-0.264	0.258	0.388	0.397	0.781	0.150
208	0.043	0.671	-0.144	0.124	0.373	0.374	0.574	0.145
209	-0.119	0.826	-0.499	0.151	0.251	0.317	0.642	0.114
210	-0.011	0.827	-0.154	0.052	0.412	0.369	0.661	0.156
212	-0.111	0.841	-0.374	0.251	0.289	0.296	0.659	0.211

213	-0.103	0.916	-0.362	0.241	0.281	0.333	0.542	0.113
214	-0.015	0.879	-0.087	0.018	0.409	0.362	0.796	0.148
215	-0.053	0.332	-0.262	0.156	0.235	0.288	0.536	0.136
217	-0.077	0.635	-0.849	0.448	0.385	0.396	0.821	0.195
219	0.001	0.925	-0.089	0.027	0.452	0.461	0.804	0.109
220	-0.043	0.892	-0.401	0.086	0.3411	0.355	0.834	0.139
221	-0.005	0.836	-0.136	0.110	0.363	0.380	0.763	0.118
222	-0.056	0.581	-0.103	0.036	0.234	0.296	0.801	0.092
223	0.003	0.899	-0.125	-0.005	0.403	0.419	0.749	0.111
228	-0.052	0.365	-0.054	0.08656	0.319	0.342	0.818	0.163
230	-0.031	0.686	-0.501	0.116	0.297	0.316	0.758	0.126
231	-0.202	0.825	-0.468	0.243	0.368	0.417	0.951	0.151
232	-0.057	0.705	-0.472	0.292	0.345	0.387	0.958	0.139
233	-0.017	0.672	-0.289	0.240	0.427	0.401	0.581	0.180
234	-0.071	0.834	-0.109	0.005	0.363	0.360	0.651	0.174

5.7.2 Amplitude and Time Plane Features Statistical Analysis

The statistical analysis of recorded amplitude and time plane features [S. Banerjee et al., 2012; I.I. Amr et al., 2010] can also be utilized to validate results for all measurements of single detected characteristic points. Standard deviations (S.D.) and coefficients of variation (C.V.) are considered in this process and calculated using Eqn. (5.5), Eqn. (5.6) and Eqn. (5.7). Here, xi denotes the ith beat and n is the total number of beats in the record.

$$\text{Mean}=\sum \frac{x_i}{n} \tag{5.5}$$

$$\text{S.D} = \sqrt{\sum \frac{(x_i - mean)^2}{n}} \tag{5.6}$$

$$\text{Coefficient of Variance (C.V)} = (\text{S.D/Mean})*100 \tag{5.7}$$

The standard deviation (SD) indicates the absolute dispersion around the mean in a data series. The Coefficient of Variation (CV) on the other hand, represents consistency and reflects dispersion within a set of data as a percentage value.

5.7.3 Results and Discussion for Feature Extraction Process

With an average accuracy of 99.12 percent, the suggested deep learner CNN classifier

classifies the samples into five categories of arrhythmias. The proposed model's sensitivity and specificity are 100% and 99.9%, respectively. The identification and detection of cardiac arrhythmia is integrated with the Internet of medical things (IoT), allowing users to monitor their health during daily activities like walking and jogging. Implementing another sophisticated security technique and improved machine, the suggested study activity's future development includes continuing to learn consideration of multiple cardiac diseases in the telecardiology area.

Features are usually divided into two types, i.e., Morphological parts and Statistical features. Morphological features include P wave duration, QRS complex, T wave, RR interval, ST slope and heart rate. The statistical features cover means, RMS, standard deviation, skewness, and kurtosis. These are the essential features we have calculated for classifying various arrhythmias.

5.7.4 Morphological Features Calculation

In this stage**,** by starting the analysis, we have been capable of extracting different morphological features. The morphological characteristics of all MIT-BIH databases are calculated, and the value of each feature is given in Table 5.9.

Table 5.9 Detected morphological features

Feature	Value
R-R interval	0.6020
QRS complex	0.3010
ST segment	0.3100
T wave	0.1870
P wave	0.1140
Heart rate	99.66

5.7.5 Statistical Features Calculation

In this stage, we have extracted various statistical features by performing the statistical analysis. These involve mean, root mean square (RMS), standard deviation (SD), skewness, kurtosis, and peak value. The mathematical calculation of statistical features is using Eqns. (5.5), (5.6) and Eqn. (5.8) given in Table 5.10.

$$\text{Mean}=\sum \frac{x_i}{n} \tag{5.5}$$

$$\text{S.D} = \sqrt{\sum \frac{(x_i - mean)^2}{n}} \tag{5.6}$$

$$RMS=\sqrt{\sum_i x_i^2} \quad (5.8)$$

Here, x_i= ith beat and n represents the total number of beats, while SD denotes the standard deviation used for the measurement of absolute dispersion in the signal. It provides the facility for the calculation of a complete dataset. Skewness (S) is used to measure the similarity of given data. The skewness has the property of perfect symmetry, i.e., the normal distribution has the value of exactly zero, defined as in Eqn. (5.9).

$$\text{Skewness} = E[x-\mu/\sigma]^3 \quad (5.9)$$

Similarly, even if a normally distributed version of the data has reached its peak or is flat, the Kurtosis (K) is used for the measurement defined in Eqn. (5.10)

$$\text{Kurtosis} = E[x-\mu/\sigma]^4 \quad (5.10)$$

The statistical features of all MIT-BIH database is calculated and the value of each feature is given in Table 5.10.

Table 5.10 Detected statistical features

Parameter	Value
Mean	0.7308
Root Mean Square value	0.732
Standard Deviation	0.0436
Kurtosis	17.594
Skewness	3.4468
Peak Value	1

5.8 Results of Classification Using Deep Learned CNN

The suggested study uses a deep learner convolutional neural network for classification, using the fully connected layer (FC) to accomplish signal classification. Table 5.11 describes the functions used in the proposed deep Learning Convolution neural network model. Then we tested the different classifiers to see whether they could improve the model's outputs. Table 5.12 Parameters of implemented deep learned CNN model and Figure 5.49 shows the block diagram for the proposed work, and Figure 5.50 shows the schematic diagram of the proposed 1D-CNN model. We

compared the results of the proposed deep learned convolution neural network (CNN) model with the results of existing electrocardiogram cardiac arrhythmia classification models, such as deep convolution neural network, support vector machine (SVM), knowledge base technique, genetic algorithm-based back-propagation Neural network, convolution neural network (CNN), bat-rider optimization algorithm-based deep convolutional neural networks (BaROA DCNN). Figure 5.51, Figure 5.52 and Figure 5.53 illustrate the calculated findings in terms of accuracy, sensitivity, and specificity.

As shown in Figure 5.54, the training set consists of diverse samples separated into five classes. The calculated values are given in Table 5.13, i.e. non-ectopic beat, supraventricular ectopic beat, ventricular ectopic beat, fusion beat, and unknown beat. Table 5.14 shows the explanation of various approaches. The proposed method is superior to existing approaches such as knowledge base technique, support vector machine (SVM), convolution neural network (CNN), deep convolution neural network (DCNN), genetic algorithm-based back-propagation Neural network (GA-BPNN), CNN+LSTM, bat-rider optimization algorithm (BaROA DCNN) and proposed method in terms of accuracy is 85.07%, 91.68%, 92.44 %, 92.34%, 92.27%, 92.26%, 93.19%, 99.12%—deep convolutional neural networks based on the bat-rider optimization algorithm (BaROA DCNN). Convolutional neural networks and long short-term memory (CNN+LSTM) are two different types of neural networks. The sensitivity of other approaches such as knowledge base technique, support vector machine (SVM), convolution neural network (CNN), deep convolution neural network (DCNN), genetic algorithm based back-propagation Neural network (GA-BPNN), CNN+LSTM, bat-rider optimization algorithm (BaROA DCNN) and the proposed method is 95%, 95%, 95%, 94.05%, 94.05%, 94.05%, 95%, and 100%, respectively, and the specificity of different approaches such as knowledge base technique, support vector machine (SVM), convolution neural network (CNN), deep convolution neural network (DCNN), genetic algorithm based back-propagation Neural network (GA-BPNN), CNN+LSTM, bat-rider optimization algorithm (BaROA DCNN) and the proposed method is 81.52 %, 89.47%, 93.22%, 93.16%, 93.08%, 93.05%, 93.9%, 99.9%.

As a result, the suggested technique outperforms existing state-of-the-art techniques such as DCNN, SVM, knowledge base technique, GA-BPNN, BaROA DCNN, and

CNN+LSTM regarding accuracy, sensitivity, and specificity. The confusion matrix for the presented CNN model is also obtained and displayed in Figure 5.55. The confusion matrix summarizes the categorization of individual classes. The matrix's diagonals draw attention to the correctly classified classes. The inaccuracy in detecting arrhythmia in our suggested model is relatively low and may also be used for efficient ECG signal processing. Finally, compared to existing approaches documented in the literature, we attained better outcomes.

Table 5.11 Description of common functions and components used in a deep learning Convolutional Neural Network (CNN) model

Function	Explanation
Conv1D	Used for conversion of 2-D to 1-D input information
Dropout	Used for prevention of over fitting problem
Batch Normalization neural networks	Reduces the internal correlation shift to accelerate deep
MaxPooling1D domain signal	Used for applying the max pooling function to a spatial
Flatten dimensional data	Used to convert multi-dimensional data input into one-
Relu	Used to perform linear rectification activation on input vector of the upper layer of neural network and produces the nonlinear output results
SoftMax neural network output	Activation function applied for multiclass classification

Table 5.12 Parameters of implemented deep-learned CNN model

Parameter	Value
Activation used	ReLU
Size of the input layer	187×1
No. of classes	7
Optimizer used	Adam
Regularization	0.1
Learning rate(λ)	0.001
Batch size	32
No. of epochs	15

Table 5.13 Summary of the classification outcomes using proposed methodology

Class	Precision	Recall	F1 score	Accuracy(%)
Non-ectopic beat	0.99	0.98	0.98	98%
Supraventricular ectopic beat	0.74	0.85	0.79	
Ventricularectopic beat	0.96	0.96	0.96	
Fusion beat	0.59	0.83	0.69	
Unknownbeat	0.98	0.99	0.99	

Table 5.14 Performance of the proposed method in comparison to existing approaches

Methods	Accuracy (%)	Sensitivity (%)	Specificity (%)
knowledge-based approach [T. Teijeiro, P. Felix, 2018]	85.07	95	81.52
SVM [S. Raj and K.C Ray, 2017]	91.68	95	89.47
CNN [X. Zhai and C. Tin, 2018]	92.44	95	93.22
DCNN [U.R. Acharya, S. Lih. Oh, 2017]	92.34	94.05	93.16
GA-BPNN [H. Li, D. Yuan et.al, 2017]	92.27	94.05	93.08
CNN+LSTM [S.Lih. Oh et.al, 2018]	92.26	94.05	93.05
BaROA –DCNN[D.K. Atal and M. Singh, 2021]	93.19	95	93.9
Deep learned CNN (ProposedMethod)	**99.12**	**100**	**99.9**

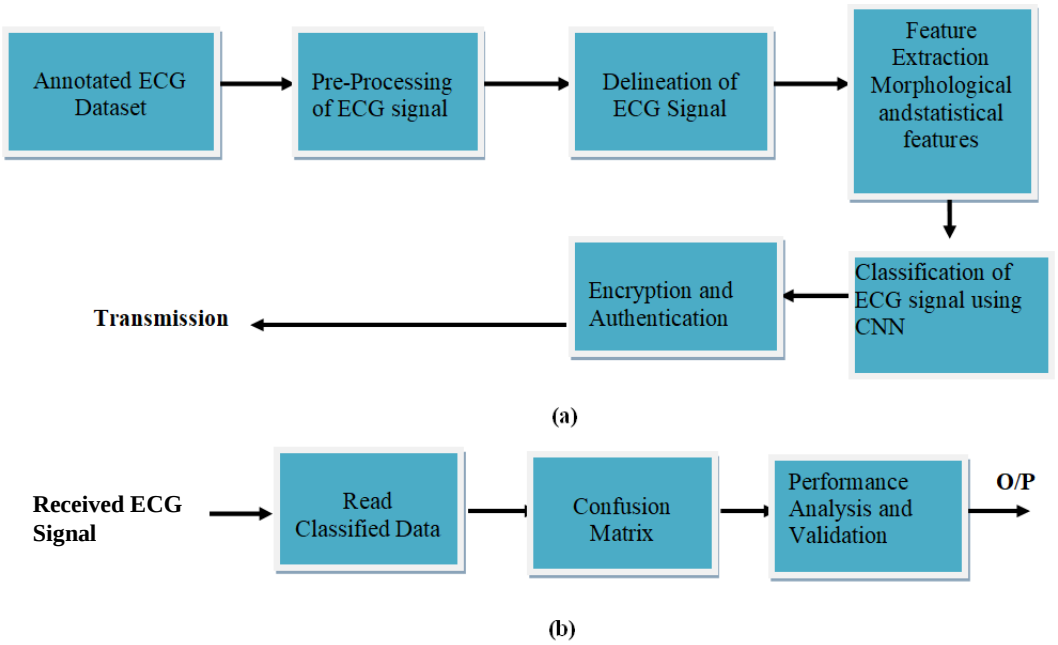

Figure 5.49 Block diagram of proposed research work (a)Transmission of ECG using Thingspeak cloud (b) Receiver

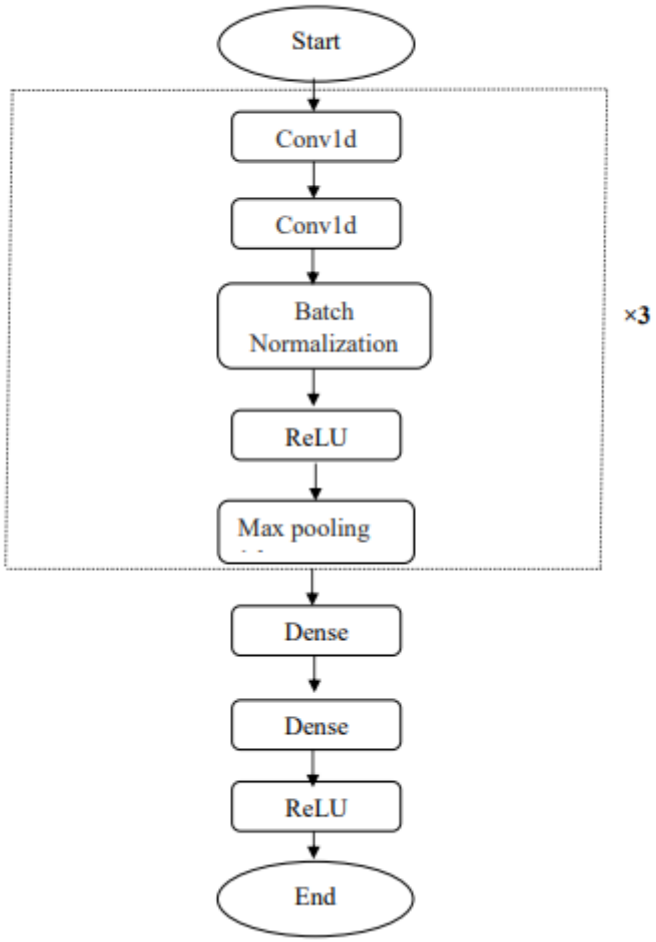

Figure 5.50 Schematic diagram of the proposed 1D-CNN model

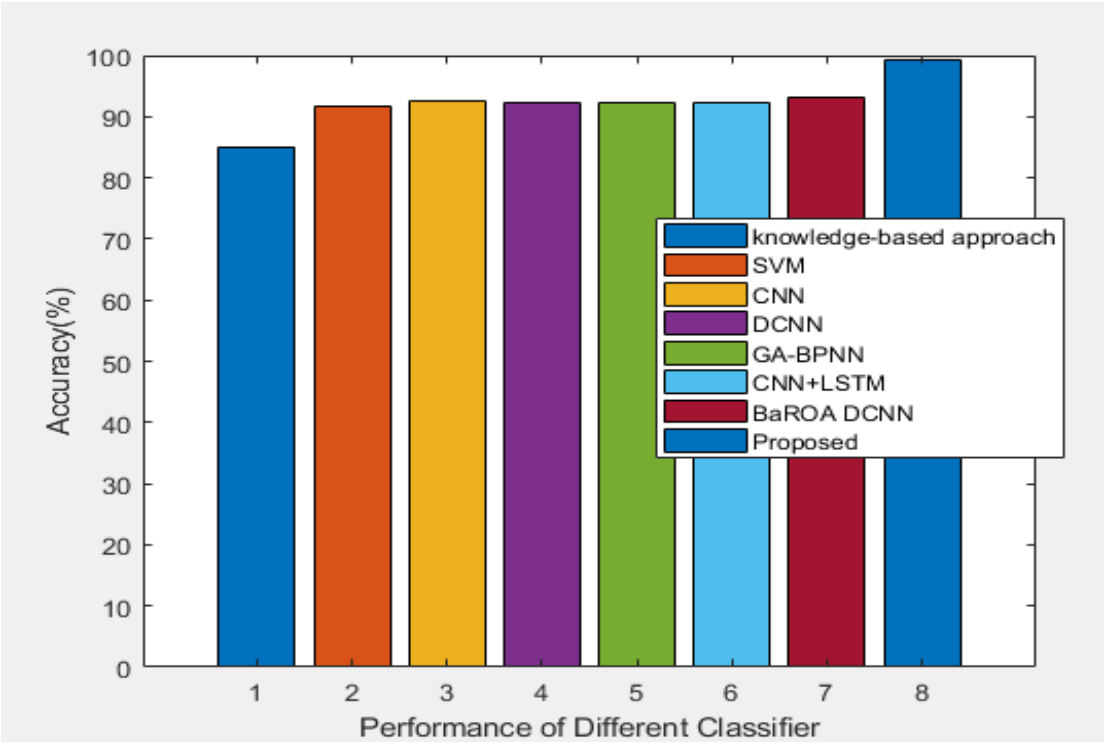

Figure 5.51 Comparison of accuracy of different classifiers

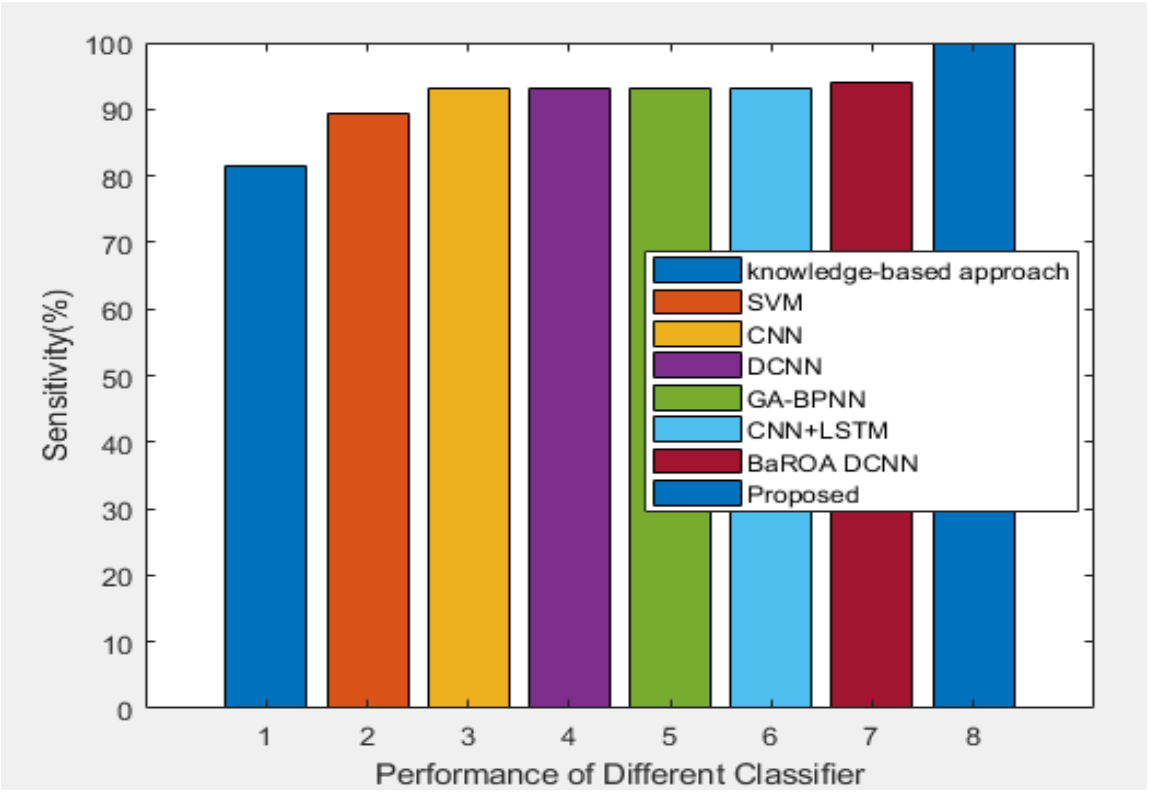

Figure 5.52 Comparison of sensitivity of different classifiers

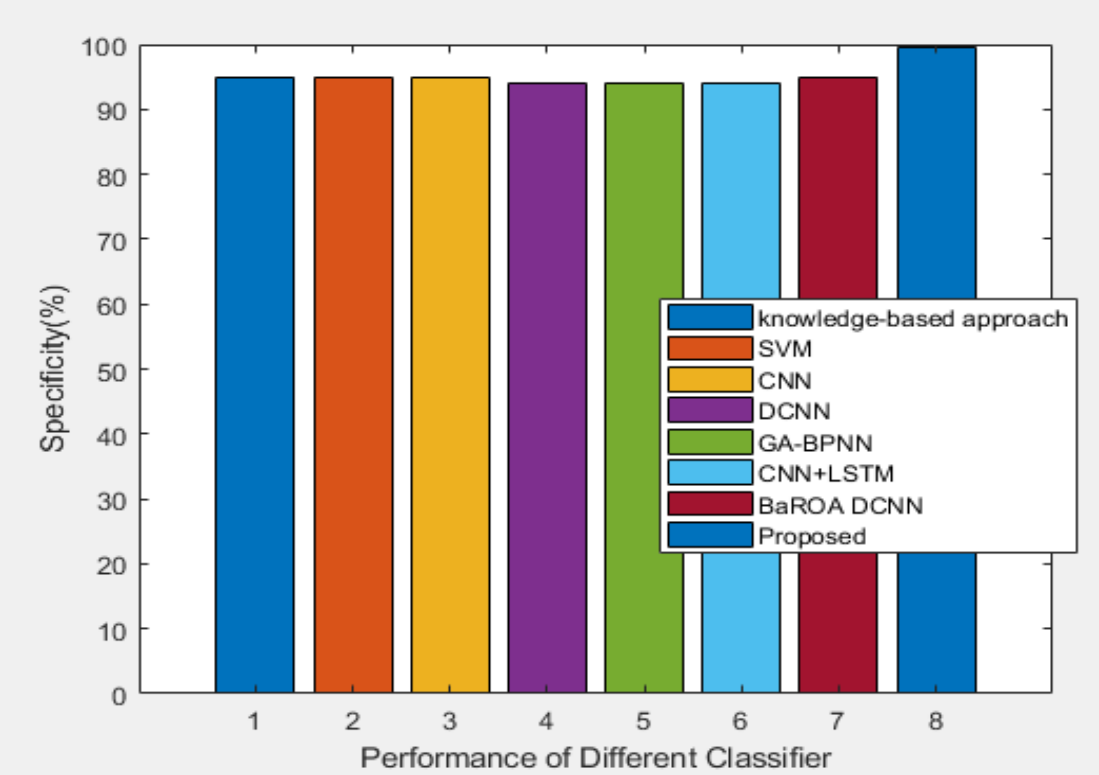

Figure 5.53 Comparison of specificity of different classifiers

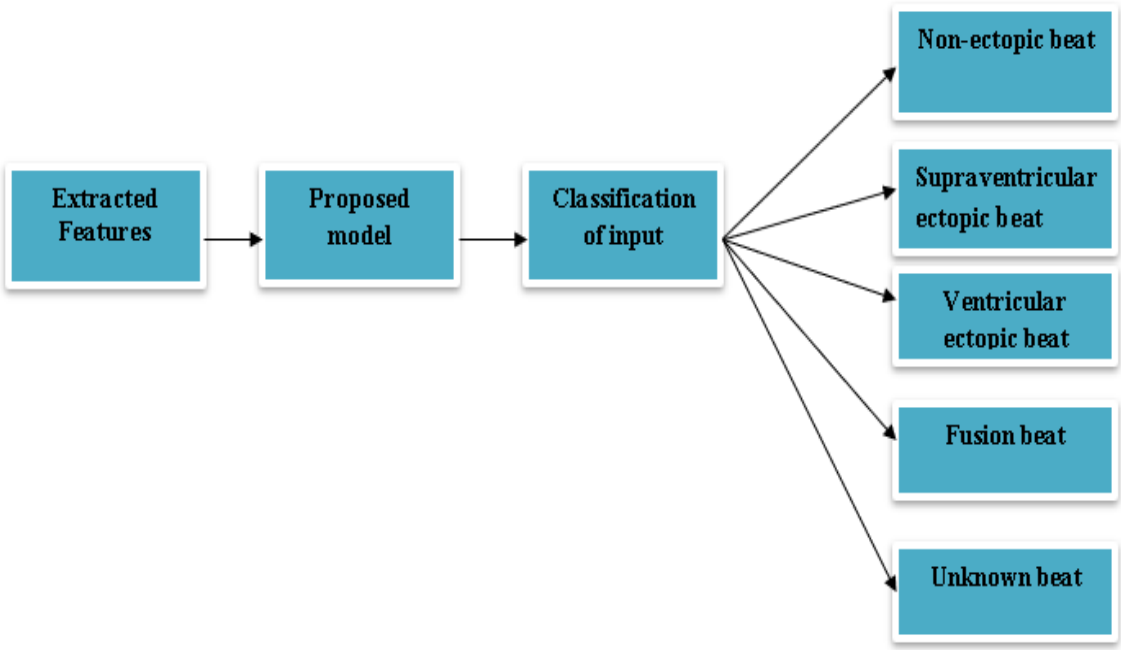

Figure 5.54 Classifications of the number of classes using the proposed deep-learnedCNN model

Figure 5.55 Confusion matrix of proposed deep-learned CNN classification model

5.9 Flow Diagram of Water Cycle Optimization Algorithm (WCOA)

- Create a random initial population using the WCOA's system parameters: dmax, Npop, max iteration, and Nsr (streams, rivers, and sea). The values of these factors used to generate the initialization vector key are shown in Table 5.15.
- Calculations of every raindrop using the fitness function (FF), determine the initial flow intensity.
- Streams lead to rivers, which lead to the sea.
- If FFstream (stream fitness function) outperforms FFRiver (river fitness function), replace the river's position with the stream's location that provides better optimum solutions.
- Replace the river's location with a sea if the FFRiver (fitness function of the river) is greater than the FFsea (fitness function of the sea).
- If the evaporation situation is satisfactory, clouds form, the rainy process begins, and the value of dmax decreases.

- Determine whether or not the convergence criteria have been met. The procedure will be terminated if this condition is met; otherwise, it will returnto step 3.

Table 5.15 WCA algorithm parameters used to generate an IV (Initialization Vector) key

Parameters	Value
Nsr	2
Dmax	$1e^{-6}$
Number of Populations	25
Total Number of iterations	100

Below is an example of WCO being used to generate the best key

Example of generated key >>

Columns 1 through 19

1 0 1 0 1 0 1 0 1 1 0 1 0 1 1 0 0 0 0

Columns 20 through 38

1 1 1 0 1 1 1 0 0 1 0 0 1 1 1 1 0 1 1

Columns 39 through 56

0 1 1 1 1 1 1 0 0 1 1 0 1 0 1 1 0 0

5.10 Complexity Time

The complexity time of an algorithm is a measure of how it behaves regardless of the platform on which it is running. The whole populations are clustered [G.A. Khan et al., 2021] into numerous frames in water cycle optimization. Instead of evaluating the information on transmission architecture between all streams, we used this feature throughout the method. When it comes to finding a comprehensive solution, the data from the ruler of every group, such as rivers or seas, is taken into account. This resulted in a significantly more effective method in terms of computation complexity. The order of complexity is n (O(n)), where n represents the size of arrays and O(n) is the linear time.

5.11 Performance Matrices

The various parameters are calculated to analyse the suggested method in comparison to currently available techniques

5.11.1 Avalanche Effect

The avalanche effect is a phenomenon in which significant changes in output data can

be measured with minimal fluctuation in input data. In an ideal world, modifying one bit in the original signal would result in a 50% change in output, and we attained the findings, which were computed using Eqn. (5.11).

$$\text{Avalanche Effect} = \frac{\text{Number of Bits Changed in the Encrypted Data}}{\text{Block Size}} \times 100 \qquad (5.11)$$

5.11.2 Mean Square Error (MSE)

One of the most widely used quality reduction metrics is Mean Square Error (MSE). Consider two signals of size N*M, X and Y, and introduce the plain image, encrypted picture, and decrypted image for each signal [M.A. Nada and A.A. Suaad, 2016]. The MSE between two ECG signals is calculated using the Eqn. below (5.12).

$$\text{MSE} = \frac{1}{N \times M} \sum_{i=0}^{N-1} \sum_{j=0}^{M-1} [X(i,j) - Y(i,j)]^2 \qquad (5.12)$$

When Y is equal to X, the MSE value is minimal, and when the Mean square error value is equivalent to 0, the value of Y is an exact duplicate of X.

5.11.3 Number of Pixels Change Rate

The Number of Pixels Change Rate (NPCR) is a technique for analyzing the difference between the input and encrypted signals. NCPR is expressed mathematically as Eqn. (5.13) [A. Alzubaidi and N.Al. Shakarchy, 2014].

$$\text{NCPR} = \frac{\sum_{i=1}^{N} \sum_{J=1}^{M} Dif(i,j)}{N * M} * 100 \qquad (5.13)$$

$$where\ Dif(i,j) = \begin{cases} 1 & I(i,j) = I'(i,j) \\ 0 & I(i,j) = I'(i,j) \end{cases}$$

I(i, j) and I'(i, j) are the initial and encrypted signals, respectively. We have completed the transmitted data at the output if the value of NCPR is now very big for the ideal encryption approach.

5.11.4 Unified Averaged Changed Intensity

The unified averaged changed intensity (UACI) analysis calculates the intensity change of the corresponding target signal's pixel location. If UACI has a high value, it can protect the encrypted approach from cyber-attacks. The Eqn. (5.14) is used to calculate it.

$$\text{UACI} = \sum_{i,j} \frac{|C^1(i,j) - C^2(i,j)|}{F.T} * 100\% \qquad (5.14)$$

$where\ C^1\ (i,j) and C^2\ (i,j)$ is the pixels value at i, j.

5.11.5 Execution Time

In seconds, it is the entire time consumed by the Electrocardiogram data during the encryption procedure. The execution time in MATLAB is computed using the tic and toc commands. In this study, we encrypt the ECG signal in the shortest period possible, 0.003 milliseconds.

5.11.6 Frequency Test

The total number of zeroes and ones for the entire sequence is the focus of the test. This test is used to see if the number of zeroes in the series is the same as expected in a random series. The main goal of this test is to determine how near the proportion of complete ones is to half value; the series should be equal. The passing of this test determines the test's entire worth. The test value that we computed is displayed in Table 5.16.

5.11.7 Run Test

The total number of runs shown in the sequence is the focus of this test. An uninterrupted series of the same number of bits is called a run. A run k has the same number of bits as the previous one and bounces with numerous opposite bits before and after. This test aims to see if the runs of different lengths of ones and zeros are as expected for a random sequence. This test determines the oscillation between zero and one or too rapid and slow. Table 5.16 demonstrates how we calculated the valuation of the passed test in this proposed work.

Table 5.16 shows the comparison of the proposed technique with traditional key generation approaches

Algorithms	Frequency Test	Run Test
Fibonacci Series	0.02	0.30
Proposed Method	0.1814	0.52

5.11.8 Comparison with Existing Approaches

The proposed work uses 3-DES and water cycle optimization techniques for encryption and authentication. Using a variety of encryption and authentication schemes, we examined the model's optimum results. One-time padding (OTP) key is required for the encryption-authentication technique. A water cycle optimization approach was used to produce a 56-bit OTP key. In contrast to the existing work, the

output demonstrates that the stenographic verification system creates a key and offers sufficient security. Symmetrical key methods are recommended over asymmetrical key techniques for ECG data transfer security. Many encryption algorithms, such as AES, DES, triple data encryption standard (3-DES), Blowfish, Rivest–Shamir–Adleman (RSA), and two fish-based encryptions, are available in the literature. Each of these algorithms has its own set of pros and limitations.

In comparison to all of these approaches, AES delivers higher security. The triple DES, on the other hand, uses less CPU. Furthermore, the triple DES was designed for embedded applications, whilst the advanced encryption standard (AES) works well for hardware and software system implementation. Similarly, the triple data encryption algorithm is compatible and adaptable with the Internet - of - things (IoT) systems.

Electrocardiogram subsystems occasionally use Bluetooth wireless protocol for the Internet of Things (IoT), and Bluetooth procedures are typically space and power restricted. Compared to AES-based techniques, 3-DES necessitates a significant storage and processing capacity. It is sometimes only appropriate for portable options (such as the Internet of Things system). In the suggested approach, we choose triple data encryption standard (3-DES) as encryption with IoT. However, advanced encryption standards (AES) should be investigated more in the future.

Table 5.17 demonstrates the results of comparing the performance of the presented triple data encryption standard (3-DES) and water cycle optimization approaches (WCO) for authentication for the security of electrocardiogram (ECG) data in a variety of ways. Avalanche effect, mean square error, execution time, number of pixels change rate (NPCR), unified averaged changed intensity (UACI), and key analysis are all included in these tables. In comparison to previous work, the significance of this suggested methodology is that it gives minimal error while requiring less time consumption, a higher avalanche effect value, NCPR, and UACI. Table 5.17 compares the development of a 56-bit one-time padding key using the water cycle optimization technique to existing key generation strategies. At a 1% level of significance, the computed key p-value is displayed. The result demonstrates that the p-value for the proposed approach is higher than 0.01. Aside from that, the water cycle optimization technique generates a 56-bit random key that is accurate. The results in Table 5.17 show that the suggested strategy is superior to existing

approaches for biological signal security, as reported in the literature.

Table 5.17 Comparison of the proposed technique to Existing Data Encryption approaches

Methods	Avalanche Effect	MSE	Execution Time	NCPR	UACI
[K.Muhammad et.al, 2018]	-	-	0.67	99.6125	33.44
[A. Kumar and G.G. Ramirez, 2018]	-	-	0.79	99.615	33.4658
[R. Hamza et.al, 2019]	-	-	0.95	99.609	33.465
[Z. Wang et.al, 2019]	50%	-	0.0027	-	-
[J. Khan et.al (2020(a)]	-	-	0.28	99.6212	33.4406
[J. Khan et.al, 2020(b)]	-	-	0.2277	99.6383	33.3516
[L. Zheng et.al, 2020]	49.28%	0.498	0.005	100	30.686
[A. Abdulbaqi et.al, 2021]	-	-	-	99.64	33.54
Proposed Method	**50.12%**	**0.4639**	**0.003**	**100**	**39.698**

5.12 Internet of Things

A system of connected devices is known as the Internet of Things (IoT). These gadgets typically include an installed framework scheme and the capacity to interact online and with other equipment. Figure 5.56 shows the block diagram of IoT Devices**.** An IoT service is one of the main parts of an overall IoT system that connects numerous 'things.' The "things" that comprise IoT systems have such an intriguing implication: they are powerless to act independently. At the very least, they should be able to connect to other "things." The true power of IoT is only realized when objects connect to help, either directly or via other "things". The server functions as an undetected manager in such setups, capable of performing tasks going from primary data gathering to complex data processing**.** This toolkit is additionally included in MATLAB programming and is accessible for download from the math work. We logged in to this IoT with a user ID and password and uploaded the data, as shown in Figure 5.57, after which it was sent to the cardiologist for further investigation.

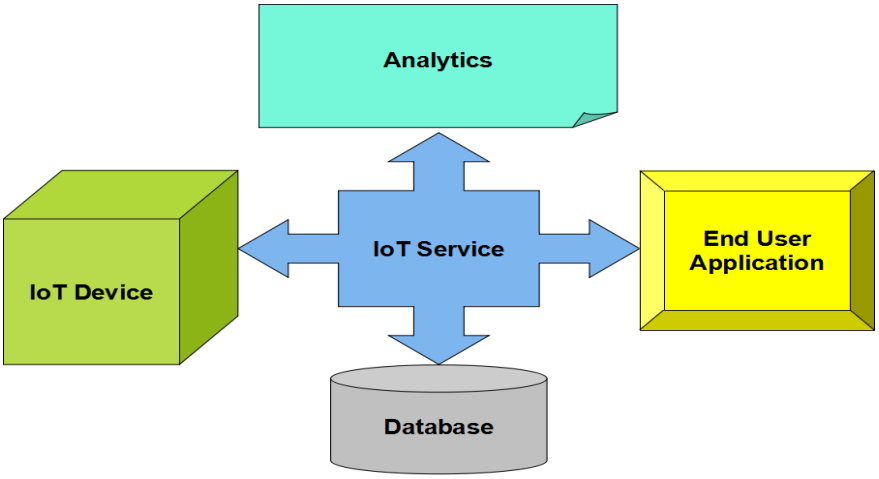

Figure 5.56 Block Diagram of IoT Devices

An Internet of Things application framework is called "ThingSpeak" which offers a range of analysis, tracking, and response capabilities. Let's take a closer look at ThingSpeak.

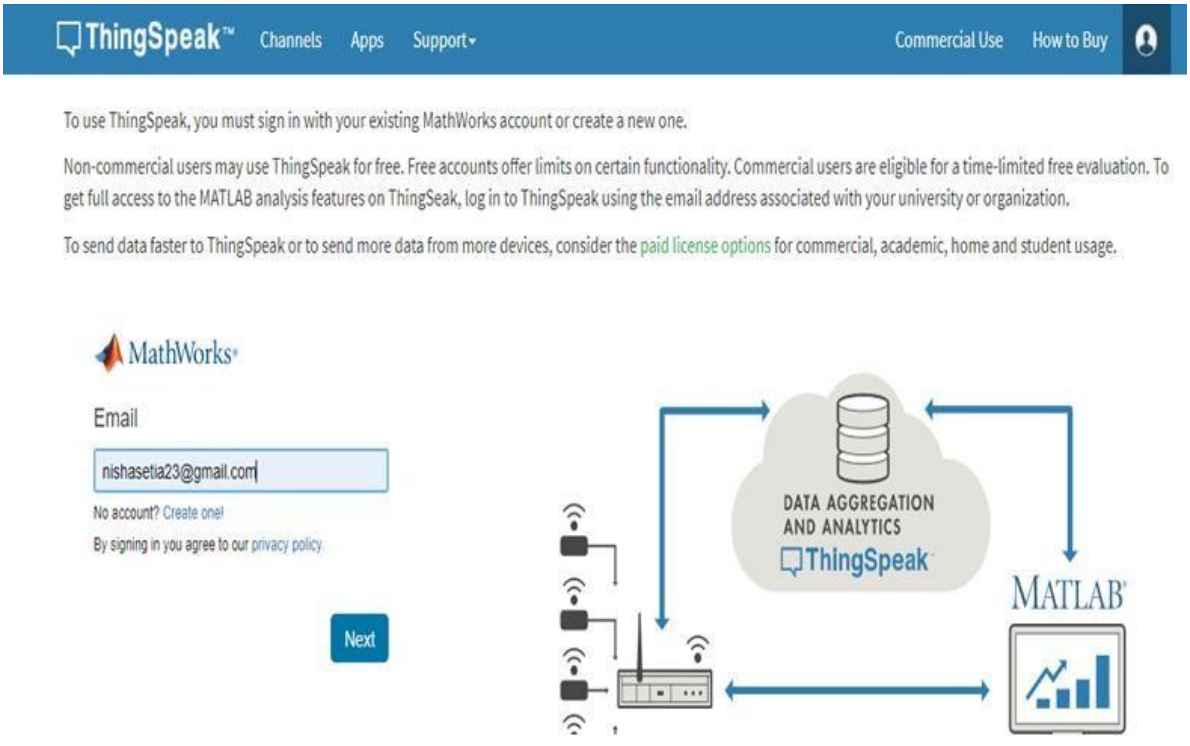

(a)

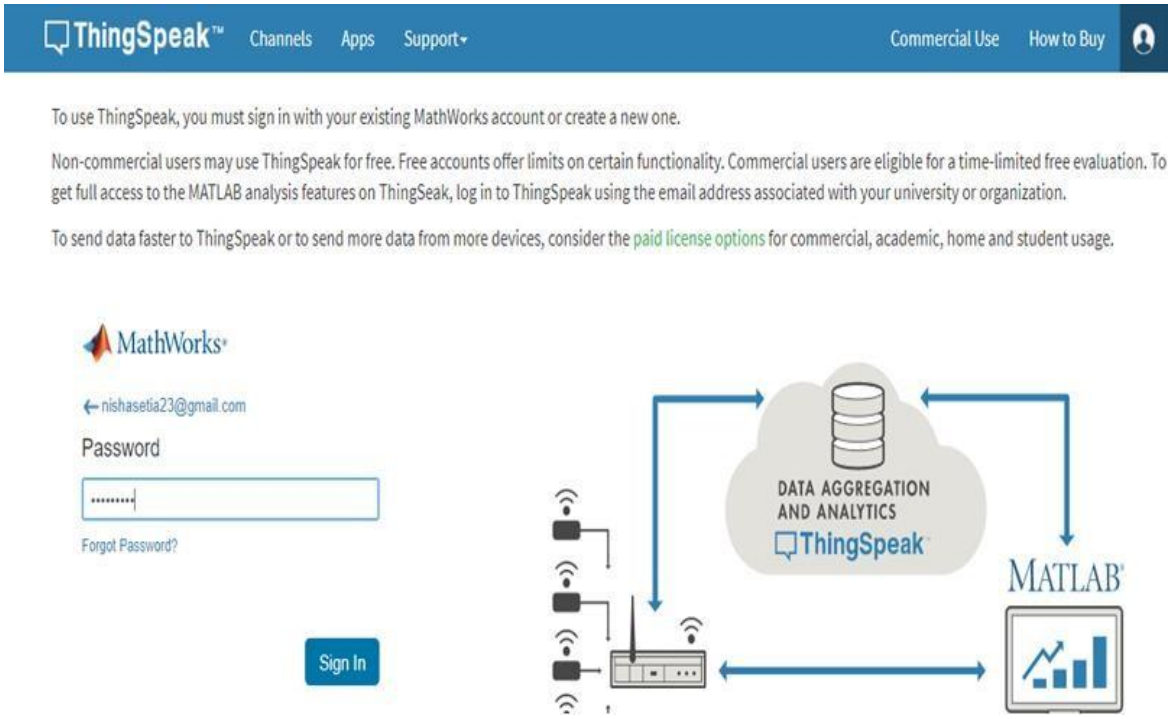

(b)

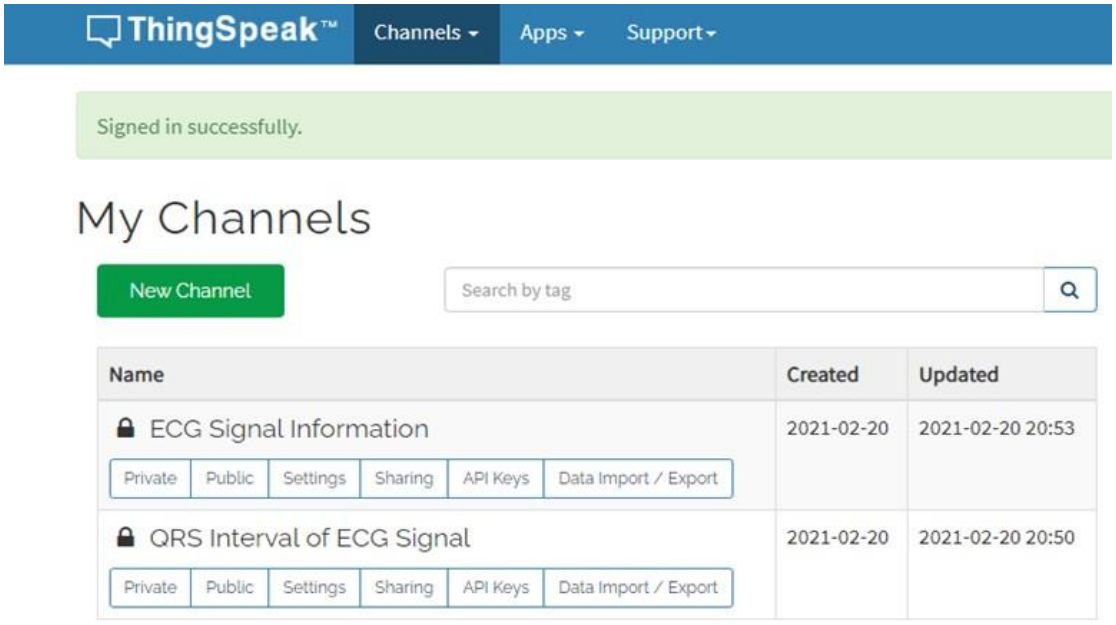

(C)

Figure 5.57 Framework of IoT (a) Login Id (b) Password (c) Upload the data

5.13 Identification of ST Deviation

The Transition region on an ECG is the region between the onset of ventricular depolarization and its conclusion. In other words, it is the distance between the QRS

complex endpoints and the starting of the T wave. The ST segment is the amount of time the cardiac muscle continues to contract to push blood out of the ventricular contraction. One of the most frequent ECG conditions brought on by ischemia is ST divergence (elevation or depression); The height and distress of the ST segment with a standard in the ECG signal are used to evaluate myocardial ischemia close to the implemented lead. Subendocardial infarction is characterized by depressed ST segments (or episodes), whereas transmural (sub-epicardial) ischemia is characterized by increased ST segments [A. Goldberger, 1981]. Figure 5.58 illustrates how the European ST-T database identified the ST- segment (Normal, Elevation) for e0103 and the depressed signal for e0105. According to our analysis of ten records' total diagnostic beat counts, the records e0103, e0104, e0105, e0108, e0113, e0114, e0147, e0159, e0162, and e0206 have four, three, three, two, one, and one diagnosis beats, respectively.

To assess each class' performance, we provided the average sensitivity and specificity for assessing advancement in the identification domain. Sensitivity and specificity are calculated using Eqns. (5.3) and (5.15).

Sensitivity is a measurement of the number of positive instances, which can be calculated as

$$\text{Sensitivity (SE)} = [TP/(TP+FN)] * 100 \qquad (5.3)$$

True positive, true negative, false positive, and false negativity, respectively, are denoted by the symbols TP, TN, FP, and FN.

However, specificity is a measure of the percentage of true negatives and is explained as

$$\text{Specificity} = TN/(TN+FP) \qquad (5.15)$$

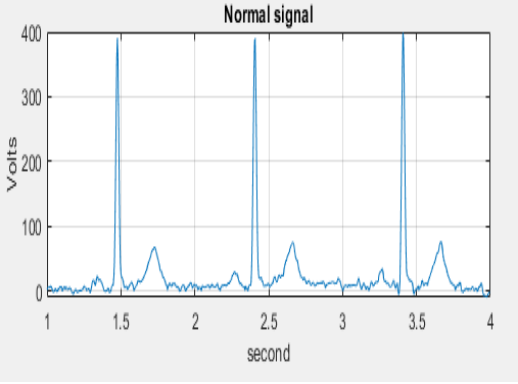

(a) Normal ST-segment

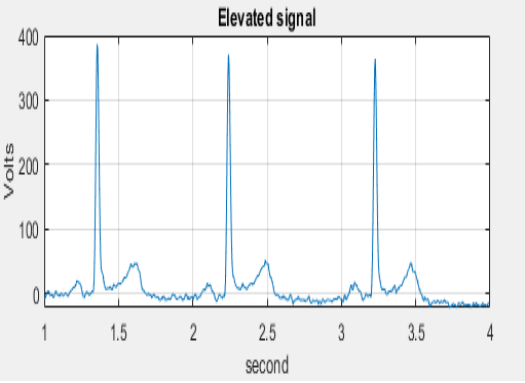

(b) Ischemic (elevated)

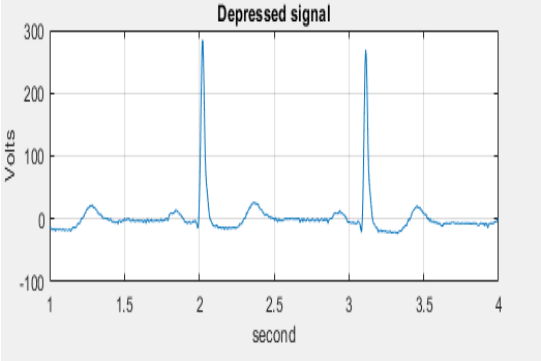

(c) Ischemic (depressed) ST segment

Figure 5.58 (a) Normal ST-segment of e0103 record of EDB (b) Ischemic (elevated) ST segment of e0103 record of EDB (c) Ischemic (depressed) ST segment of e0105 record of EDB.

5.14 Comparison with Existing Approaches

The isoelectric energy measurement function, which does not involve any complicated computations, is presented in this study as a new modified function for diagnosing ischemia. Using the entries mentioned above from the EDB database, the outcome of the methodology was contrasted to that of the existing technique. This dataset employs a classification scheme for ischemia pulses. Ischemic beats were expected to be present in every annotated record in the dataset. Many perspectives [N. Maglaveras et al., 1998] cannot be compared because they used different databases or used other outcome metrics or datasets. HMM [R.V. Andreao et al., 2004] produces a good classification for detecting ischemia episodes; it is worthless for non-invasive events. [M.G. Tsipouras et al., 2007] study on fuzzy logic Based systems are crucial for rule analysis' prognosis of infarction, but additional study is needed to enhance detection efficiency. The researchers' findings are as follows: both the sensitivity (SE) and specificity (SP) are, on average, 91.2% and 90.9%.

In this study, the researchers found that the average sensitivity (SE) and specificity (SP) were 81% and 84%, respectively. This is demonstrated by the genetic algorithm [C. Papaloukas et al., 2004], the support vector machine [J. Park et al., 2012], and kernel density estimation [S. Don et al., 2013]. Cardio dynamics gram is a model technique for the timely detection of heart failure [C. Wang et al., 2016]. Standard 12-lead ECG reveals myocardial ischemia. A recently designed stochastic learning technique extracts cardio dynamic information from ST-T segments. Examining

patients with ischemia using the CDG method results in a sensitivity of 90.3% and a specificity of 87.8%. [A.K. Manocha et al., 2016] proposed a technique for predicting ischemia events using statistical variables extracted from ECG ST-segment anomalies. In ischemia events, the window categorization algorithm was created to remove erroneous beats. The coefficient of variation (COV), kurtosis, and form factor are utilized to locate ischemia events. The results show an average sensitivity (Se) of 98 percent and a positive predictivity (+P) of 97 percent for 90 records from the EDB collection. [K. Nakajima et al., 2018]. Researchers reprogrammed an artificial neural network using a Japanese prospective longitudinal dataset to identify ischemia. Patients who seemed to have neither cardiac rehabilitation nor old infarction had an AUC of 0.88 for version 1.1 (sensitivity 88%) and 0.88 for version 1.0 (specificity 100%) (p =0.0093): Version 1.1 produced 0.1 to 0.7 transitional ANN probability. The T-wave area curve was proposed by [R. Li et al., 2021] as a tool for diagnosing MI (TWAC). By observing and analyzing clinical data, it was shown that there is a significant link between TWAC morphology and MI. The sensitivity, specificity, and accuracy of the presented technique in this study for identifying MI are 84.3, 83.6, and 84%, respectively. Convolutional neural networks (CNN) were proposed by [M.R. Bigler et al. 2021] as a deep learning process for extracting data-derived characteristics and acknowledging normal shapes. Consequently, Convolutional neural networks provide a balanced viewpoint on systemic diseases such as ischemia. The following results were obtained by the researchers utilizing cardiac stability or blockage as a criterion for the absence and presence of myocardial ischemia: sensitivity is 80%, and specificity is 92% at a frequency (cut-off) of 0.279 mV. This study utilized ST-segment deviations to calculate the isoelectric energy measuring function; however, additional ST-segment morphological features might also be applied. The suggested method has two significant advantages. The technique can be employed to evaluate the outcomes. This is essential for developing a system of clinically supported medical decision-making. It may be beneficial for CCU patients who lack recommendations. Secondly, instead of a complicated algorithm, straightforward analysis based on isoelectric energy is used, and the features extracted are then transferred to physicians via telecardiology for appropriate heart condition analysis that has yet to be identified in the current state of artworks. The average sensitivity (SE) is 98.5% after using this recommended approach. The average predictivity (P) is 98.3%, in contrast. These outcomes perform better than other

techniques discussed in the literature, as given in Table 5.18.

Table 5.18 shows the comparison of the outcomes of ischemia detection using the proposed method versus existing approaches

Methods	Sensitivity (%)	Specificity (%)
M.G. Tsipouras et.al, 2007	91.2	90.9
C. Papaloukas et.al, 2004	81	84
C. wang et.al, 2016	90.3	87.8
A.K. Manocha et.al, 2016	97.71	96.89
M.R. Bigler et.al, 2021	80	92
Proposed Method	**98.5**	**98.3**